Journal of Achievements in Materials and Manufacturing Engineering
VOLUME 37
ISSUE 2
December
2009

Structure and properties of the gradient tool materials based on a high-speed steel HS6-5-2 reinforced with WC or VC carbides

L.A. Dobrzański , A. Kloc-Ptaszna*
Division of Materials Processing Technology, Management and Computer Techniques in Materials Science, Institute of Engineering Materials and Biomaterials, Silesian University of Technology, ul. Konarskiego 18a, 44-100 Gliwice, Poland
* Corresponding author: E-mail address: anna.kloc@polsl.pl

Received 20.09.2009; published in revised form 01.12.2009

Materials

ABSTRACT

Purpose: This paper concerns manufacturing and researching a new group of the gradient tool materials, manufactured by a conventional powder metallurgy method, consisting in compacting a powder in a closed die and sintering it.
Design/methodology/approach: The materials were obtained by mixing the powders of the HS6-5-2 high-speed steel, tungsten carbide (WC), and vanadium carbide (VC). The mixes were poured one by one into the die, yielding layers with the gradually changing volume ratio of carbides within the high-speed steel matrix. Structural research by using the scanning and transmission electron microscopes, x-ray microanalysis and density, hardness and porosity tests, were performed. Structure and hardness of selected materials after heat treatment were also investigated.
Findings: On the basis of the results of the research, it was found that it was possible to obtain gradient materials by the powder metallurgy methods, in order to ensure the required properties and structure of the designed material. It was shown that the new sintered graded materials were characterized by a multiphase structure, consisting of ferrite, primary carbides of the high speed steel, of the MC and M_6C type, and dependently of the reinforcement phase, of the tungsten carbide WC or the vanadium carbide VC, which were introduced into the material, in the form of powder. Additionally in the structure of the WC-reinforced materials the W_2C phase occurs. The gradient tool materials reinforced with the WC carbide were characterized by a higher hardness, and a lower porosity in relation to the materials reinforced with the VC carbide. It was found that the desired structure and properties (density, porosity and hardness) had the material containing 25% of the WC carbide in the surface layer, after sintering at the temperature 1210°C, for 30 minutes. The heat treatment application causes a significant increase of the surface layer hardness of the material. The highest surface layer hardness, equal to 71.6 HRC, shows the material austenitized at the temperature 1120°C, hardened and tempered twice at the temperature 530°C.
Practical implications Developed material is tested for turning tools.
Originality/value: The material presented in this paper has layers consisting of the carbide-steel with growing hardness on one hand, and the high-speed steel, characterized by a high ductility on the other.
Keywords: Gradient tool materials; Uniaxial pressing; Sintering, High-speed steel; Tungsten and vanadium carbide

Reference to this paper should be given in the following way:
L.A. Dobrzański, A. Kloc-Ptaszna, Structure and properties of the gradient tool materials based on a high-speed steel HS6-5-2 reinforced with WC or VC carbides, Journal of Achievements in Materials and Manufacturing Engineering 37/2 (2009) 213-237.

1. Introduction

More and more demands are made to the contemporary tool materials; therefore, the need for search of new materials and technologies grows. The quest for such materials is ongoing in the last years that combine the relatively high core ductility with the high abrasion wear resistance of their surface. High-speed steels, sintered carbides, special ceramic materials, and the superhard materials, like boron nitride and diamond, are of the most importance among materials used for cutting tools [1-3]. Materials were mentioned herein-above in the order of their growing hardness criterion or of their decreasing plastic properties. Therefore, the common feature of various materials is that their high hardness is combined with their relatively low ductility. On the other hand when the high cracking resistance (ductility) is ensured their hardness is low. The research is carried out to solve this problem focused on development of materials with the layered structure, ensuring the required properties of the surface and substrate. Materials like that are fabricated, among others, with the thermo-chemical-, CVD, and PVD methods [3-6]. Layered materials, however, demonstrate certain limitations connected, among others, with the poor adhesion of the developed layers, or with the excessively high stresses between the surface layer and substrate, which results in the premature roughing or spalling of the layer [7]. Therefore, further research should be focused on materials fabrication of characteristic structure which will ensure elimination of the above-mentioned disadvantages of the layered materials. Gradient materials are these that meet the criterion mentioned above, whose properties change gradually in the material volume, along with the change of chemical composition, grain size, structure or atomic order [8-10].

Employment of the gradient materials concept may pave the way for introduction of the new materials used for cutting tools – *tool gradient materials (TGM)*.

Several main gradient materials fabrication methods were developed to date, like: powder metallurgy methods, coating deposition methods, and methods based on diffusion phenomenon [8, 11-19]. Material's gradient structure may be obtained, among others, by strengthening the matrix with precipitations or particles with various properties, sizes, and shapes, with the portions changing in the material volume [8-10]. Powder metallurgy is the method making it possible to implement relatively easily the distribution control of the reinforcing phase's particles in the matrix, ensuring full use of the feedstock, and very high repeatability of the obtained results. This method makes it possible to combine various components to obtain the required material properties that cannot be obtained economically by other methods. Many research projects pertaining to the sintered materials indicate that materials with the precisely specified chemical composition and high purity can be obtained thanks to powder metallurgy method [20-40]. Fabrication of sintered materials is divided into three main stages, i.e., fabrication of powders, forming of powders, and sintering [41]. There are many powder forming methods, like die uniaxial compacting, cold isostatic pressing of the polymer-powder slurry, vibratory forming and additional compaction in a closed die and sedimentation forming. As it turns out from the literature review, forming by filling and compacting powders in the die is the most common powder forming method in laboratory conditions [41-44]. This method is easier from the technological point of view in realisation compared to other forming methods. Moreover, this method can be easily applied in industrial conditions using conventional presses. Materials with smooth structure porosity may be obtained by pouring the mixture of powders with diverse shape of their particles or by a change of compaction conditions. However, obtaining materials by changing pores size may be obtained by varying the powder particles sizes. One can also obtain the material structure characteristic of a smooth change of chemical- and phase compositions using the powder metallurgy method, by pouring mixtures with various portions of matrix material powders with powders of material that would have to perform strengthening function [45-46]. If differences of portions of the relevant phases in the particular layers are small, due to phenomena occurring during sintering (diffusion among others) there are no clear boundaries between particular layers and structure of the obtained material that is characteristic of smooth changes of portions of the particular phases. Researches pertaining the sintered tool gradient materials are ongoing in various research centres at home and abroad, among them also in the Department of Materials Processing Technology, Management, and Computer Techniques in Materials Science of the Institute of Engineering Materials and Biomaterials of the Silesian University of Technology. The non-alloy-, low-alloy-, and medium-alloy steels were investigated using surface layers with increased portion of high-speed steel [20-24], sintered high-speed steels reinforced with carbide phases [25,45], sintered stainless steels reinforced with niobium carbides [46], and sintered carbides with varying binder portion [34]. The results obtained indicate that thanks to the powder metallurgy method it is possible to fabricate materials characteristic of structure varying in the material's volume along with its chemical- or phase composition change. Therefore, the metal powder metallurgy method consisting in the uniaxial compacting of the powder in the closed die, with its subsequent sintering, seems to be advantageous for fabrication of the new gradient tool materials.

Material with the relatively high core ductility and high surface hardness, and consequently high abrasion wear resistance, is the tool material sought. Therefore, the gradient tool materials should be designed to ensure the high abrasion wear resistance in the working layer, retaining the ductile core, making the high dynamic loads withstood possible. Literature review pertaining to tool materials suggests that the highest plasticity is characteristic of the high-speed steel from among all tool materials mentioned above. Importance of the high-speed steels remains still high in spite of the intensive development of other groups of tool materials. Moreover, development of the manufacturing technology – employment of powder metallurgy methods – has been added to improvement of service properties of the discussed steels. Thanks to the fine-grained structure characteristic of the uniform distribution of the primary carbides, and lack of carbides separation and banding, as for the conventional high-speed steel, the ductility of the steel sintered after hardening and tempering is higher than ductility of steel fabricated with conventional method. Therefore, the sintered high-speed steels feature dominates a group of used tool materials when especially desired property of the sintered tool material is its relatively high ductility [1-5].

The second desirable property of the tool material sought is its high hardness, which should exceed hardness of the machined

material by at least 30 HRC [3]. Sintered carbides, among the tool materials, are characteristic of the relatively high hardness (1900-2500HV). However, the significant brittleness of these materials limits their applications range because of the dynamic external loads occurring in service of the cutting tools [47]. High-speed steel matrix composites are characteristic of intermediate properties between the high-speed steels and sintered carbides. These materials are included into the group of sintered composites with metal matrix reinforced with particles. An advantage of the cermets is the fact that their mechanical properties can vary in a broad range depending on the matrix type and heat treatment state [3, 44, and 47]. Research ongoing currently in various scientific centres is focused on fabrication of composites based on the high-speed steels with improved abrasion wear resistance. Addition effect of WC, TiC, VC, and NbC carbides on structure and properties of the HSS matrix based composites was investigated in papers [12, 48-50]. It was found out that along with relative volume increase of carbides in the high-speed steel matrix composites their hardness and abrasion wear resistance grow; however, their bending strength decreases. One should also take into account that the secondary hardness effect occurring during tempering of the high-speed steels, connected with precipitation of dispersive carbides in the martensitic matrix and transformation of retained austenite during high-temperature tempering, which may feature an additional precipitation hardening mechanism of gradient materials, apart from the dispersive hardening by increased portion of reinforcing phases particles.

Keeping in mind all factors mentioned above, beginning of research was assumed to be purposeful pertaining to development of the new group of the high-speed steel matrix composites, reinforced with hard WC or VC carbide phases, development of their fabrication technology as well as determining their structure and properties.

2. Material for investigation

Powders of the HS6-5-2 high-speed steel, tungsten carbide (WC), and vanadium carbide (VC) were used for fabrication of the gradient tool materials. The particles of the HS6-5-2 high-speed steel, VC and WC powders particles are shown in Figure 1. Chemical compositions and main properties of these powders are presented in Table 1.

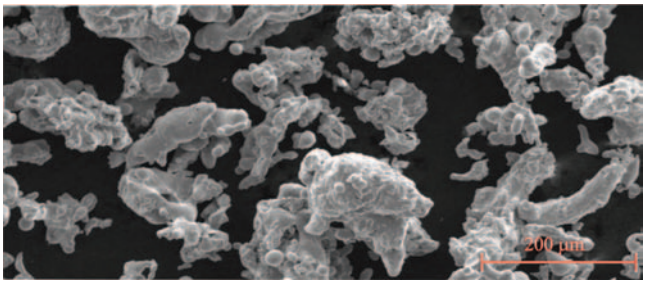

Fig. 1. Scanning electron micrographs of HS6-5-2 water atomized powders

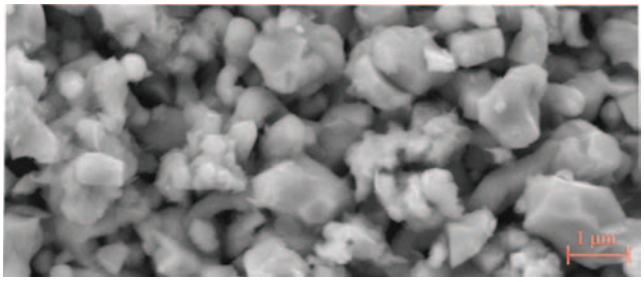

Fig. 2. Scanning electron micrographs of VC powders

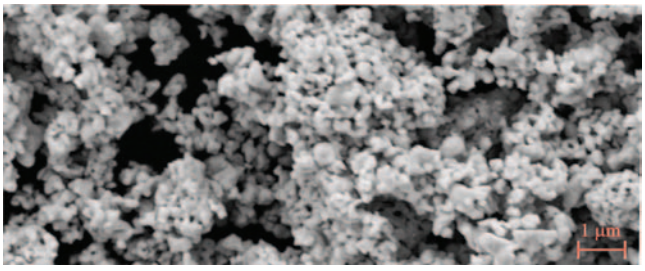

Fig. 3. Scanning electron micrographs of WC powders

Table 1.
Properties and chemical composition of powders

	Mass concentration, [%]		
Element	HS6-5-2	VC	WC
C	0.75-0.90	16.94	6.11
Mn	0.20-0,45	-	-
Si	≤ 0.45	≤ 0.01	≤ 0.002
P	≤ 0.04	-	-
S	≤ 0.04	≤ 0.008	0.003
Cr	3.75-4.5	-	-
Ni	0.2	-	-
Mo	4.5-5.5	-	≤ 0.001
W	5.50-6.75	-	rest
V	1.6-2.2	rest	0.19
Co	0.1	-	-
Cu	0.1	-	-
Fe	rest	≤ 0.05	0.003
Ca	-	≤ 0.01	0.003
Al	-	≤ 0.01	≤ 0.002
Mg	-	-	≤ 0,001
K	-	-	≤ 0.001
Na	-	-	≤ 0.001
C free	-	0.14	0.02
Grain size, µm	> 150	> 1.8	> 0.86
Additional information	High-speed steel powder, atomised with water, made by HOEGANAES	Vanadium carbide powder made by Baildonit	Tungsten carbide powder made by Baildonit

3. Investigation methodology

The investigation was carried out in three stages. The optimum concentration was selected at the first stage for the particular constituents of the surface layer of the designed materials, using the same sintering parameters (sintering temperature, T_s=1250°C; sintering time, t_s=60min). The second stage consisted in fabricating materials with the discrete gradient of the chemical composition, optimisation of the sintering parameters, as well as in examination of structure and testing of mechanical properties of gradient materials in the sintered state. Based on structure observations and examinations as well as on test results of density, hardness, and porosity, optimum concentrations of the constituents were selected in the particular material layers. At the third stage a batch of test pieces was made for heat treatment and for testing of mechanical properties and examination of the gradient material in the quenched and tempered states.

3.1. First stage

The first stage included selection of the particular constituents' optimum concentrations in the gradient material surface layer. Sintered high-speed steel matrix composites were fabricated to this end with the HS6-5-2 high-speed steel matrix reinforced with the WC tungsten carbide or VC vanadium carbide (Figure 4).

The test pieces were fabricated with the conventional powder metallurgy method, consisting in compacting the powder in a closed die and finally sintering it. The powders were mixed in relevant proportions for an hour in the WAB-TURBULA-type T2F agitator.

Compaction of powders was carried out in the uniaxial, unilateral die at the pressure of 500 MPa. The sintering was carried out in the Carbolite pipe furnace with the maximum sintering temperature of 1450°C and pressure lowered to ca. $8 \cdot 10^{-5}$ Pa and in the pipe furnace with the atmosphere of flowing N_2+5%H_2 mixture of gases. The compacts were sintered at temperature T_s=1250°C, for t_s=60min. The heating up and cooling down rate to the sintering temperature is 5°C/min. Sintering parameters were selected experimentally based on previous research [21].

Based on observations of structure of the sintered materials on the scanning electron microscope (SEM) equipped with the back-scatter electrons detector (BSE) and the dispersive energy analyser (EDAX D4) the phase composition was determined (weight and atomic concentrations of the metallic elements) in the selected micro-areas of the matrix and carbides on transverse sections of the test pieces and four single-layer test pieces were selected with the following WC tungsten carbides and VC vanadium carbides concentrations: 90 HSS/10WC, 90 HSS/10VC and 75 HSS/25WC, 75 HSS/25VC, where: HSS- HS6-5-2 high-speed steel, WC – tungsten carbide, VC – vanadium carbide; a number next to HSS, WC, and VC designates percentage volume portions of the constituents.

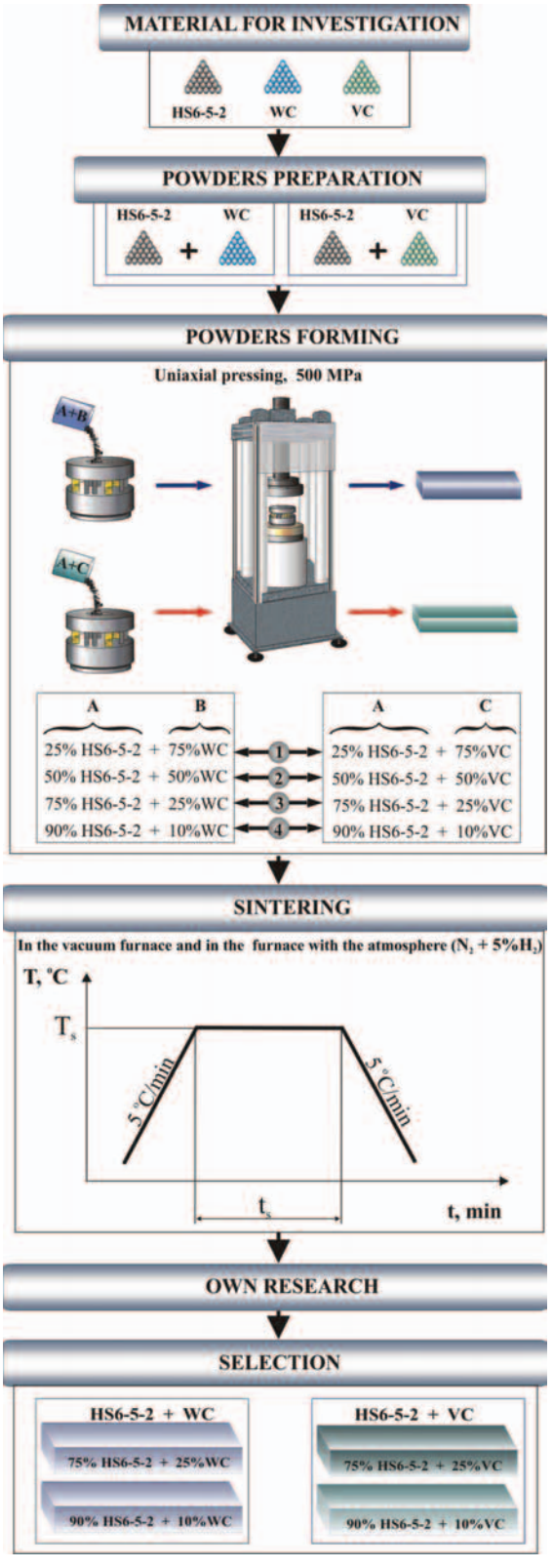

Fig. 4. The first stage

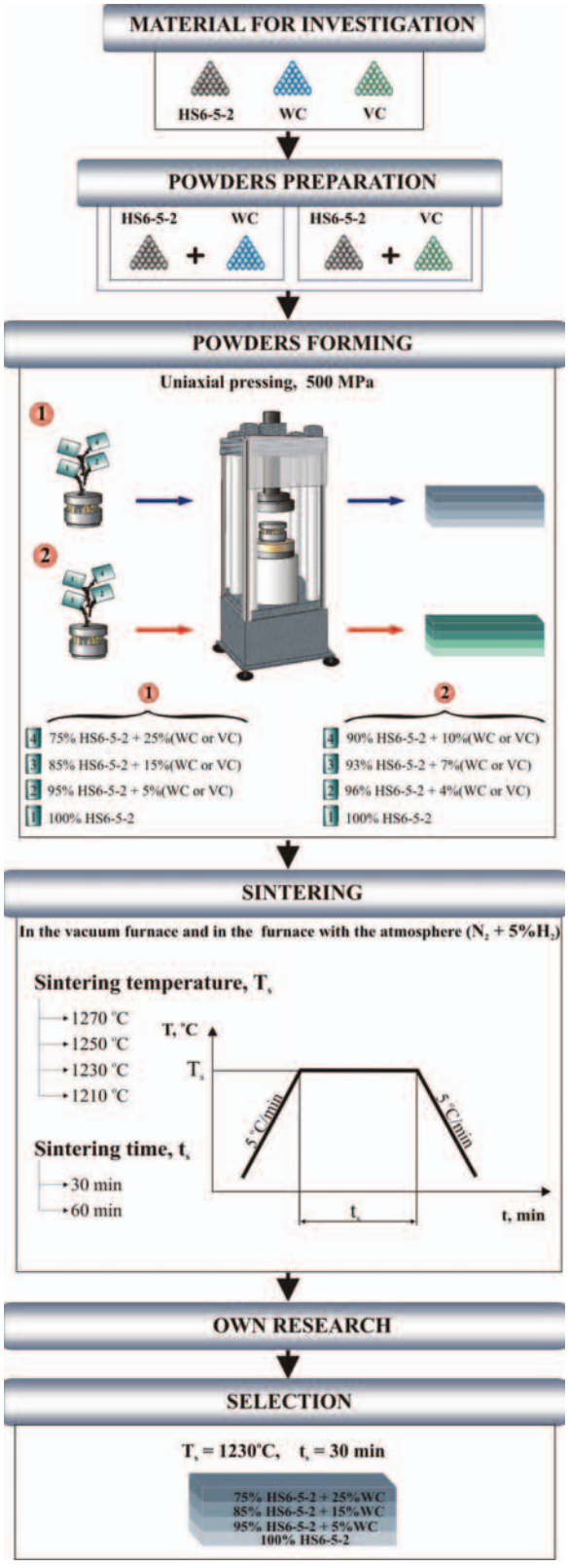

Fig. 5. The second stage

3.2. Second stage

The second stage concerned fabrication of the tool gradient high-speed steel matrix composites with the surface layers selected experimentally at the first stage (Figure 5). Four types of green compacts were fabricated with four layers. Surface layers contain 90HSS/10WC, 75HSS/25WC, 90HSS/10VC, 75HSS/25VC. The consecutive intermediate layers were constituted from the surface layer side, with the decreasing concentration of the WC tungsten- or VC vanadium carbides, down to the substrate layer containing the high-speed steel only. It was assumed that such composition of layers may correspond to the material intended for fabrication of the turning tools.

Powder mixes were poured one after the other into a die yielding layers with the gradually changing percentage volume portions of carbides in the high-speed steel. For concentration in the surface layer of 25% WC or VC the next intermediate layers were constituted containing 15% and 5% of these carbides respectively. In case of the surface layer with the 90HSS/10WC, 90HSS/10VC composition, the intermediate layers contain 7% and 4% WC or VC respectively.

The test pieces were compacted under the pressure of 500 MPa. Selection of the sintering parameters was made experimentally by variation of the green compacts' sintering temperature, time, and atmosphere. The test pieces were sintered in the vacuum furnace and in the furnace with flowing atmosphere of nitrogen with addition of N_2 + 5% H_2, at the temperatures of 1210, 1230, 1250, and 1270^{o}C, for 30 and 60 minutes.

Based on analyses carried out the gradient material was selected for further investigations with the high-speed steel reinforced with the WC tungsten carbide with the 75HSS/25WC surface layer composition.

3.3. Third stage

At the third stage a set of test pieces was prepared to carry out their heat treatment. The powders were mixed for an hour. Four consecutive layers were poured into a die, with the relevant compositions from the 75HSS/25WC surface layer, through the 85HSS/15WC, 95HSS/5WC intermediate layers, up to the high-speed steel alone. The compaction was carried out under the pressure of 500 MPa. Sintering was carried out at the temperature of 1210^{o}C for 30minutes. The heating up and cooling down rate to the sintering temperature was selected experimentally and it is equal to 5^{o}C/min. The sintered test pieces were subjected to heat treatment. The heat treatment conditions are presented in Table 2.

Table 2.
The heat treatment conditions

T_a – austenitizing temperature, ^{o}C	t_a - austenitizing time, s	$T_{tI,II}$ – tempering temperature I and II, ^{o}C
1120	80	470
1150	120	500
1180	160	530
1210		560
		590

4. Internal research

4.1. Structure examinations

Metallographic examinations were made on microsections of sintered and heat treated test pieces. Test pieces were cut in the plane perpendicular to the outer layer on the 'Isomet-4000' (BUEHLER) cut-off machine using water jet cooling. Next they were hot-mounted in the thermosetting resin, ground using the abrasive papers with the 180-2400 μm/mm^2 grain size at 300 rpm, and buffed on diamond compounds at 150 rpm.

Microsections of the sintered test pieces were etched in nital (3% solution of nitric acid in ethanol) making observations possible of the light, non-etching carbides on the dark etched matrix; whereas, microsections of the hardened test pieces were etched in the etchant containing 5 g picric acid, 100 ml purified water, 0,5 g sodium alkylsulfonate, to reveal the primary austenite grains boundaries.

Metallographic examinations were made on the light microscopes (Leica MEF4A and OPTON Axiovert) at magnifications from 100 to 1000 x, and on the scanning electron microscopes (Philips XL30 and Zeiss Supra 35) equipped with the secondary electron detectors (SE) and back scattered electron detectors (BSE or QBSD) at the accelerating voltage from 5 to 20 kV, at magnifications from 50 to 10000 x.

The primary austenite grain size was measured with Snyder-Graff method.

Volume portions of carbides were determined with the quantitative metallography methods using the Image-Pro Plus computer image analysis computer system.

The quantitative and qualitative X-ray micro-analysis and the analysis of surface distribution of the alloying elements were made on the ground and buffed microsections of the surface layers of the sintered gradient high-speed steel matrix composites on the scanning electron microscope (Philips XL30) at the accelerating voltage of 20 kV, equipped additionally with the energy dispersive X-ray analyser (Philips EDAX D4). Based on the X-ray micro-analysis chemical composition was determined (mass- and atomic concentrations of the metallic elements) in the selected micro-areas of the matrix and carbides on transverse sections of the gradient carbide alloyed composites.

Assessment of phase compositions of powders, compacts, and gradient high-speed steel matrix composites in the sintered - and heat treated states was carried out using the PANalytical X'PertPRO X-ray diffractometer using the filtered K radiation of the cobalt lamp at 40 kV voltage and 30 mA heater current. The reflected radiation intensity measurements were made in the 2θ angle range from 30 to 120° every 0.05° and counting time of 10 seconds.

The retained austenite volume portion was calculated using software developed in the Department of Materials Processing Technology, Management, and Computer Techniques in Materials Science. The software makes it possible to calculate the volume portion of the retained austenite in steels with the Averbach-Cohen roentgenographic method based on measurement results of the complete intensities of diffraction maxima of the X-ray radiation from the γ and α phases lattice planes. It was assumed in calculations that the X-ray radiation intensity deflected on the crystallographic planes of γ and α phases is proportional to the portions of these phases in steel. The Averbach and Cohen direct comparizon method, based on this assumption, requires measurement of the total intensity of two or a bigger number of diffraction maxima of α and γ phases, while α phase features the standard for austenite [52-54]. With these assumptions and taking into account the portion of carbides in the high-speed steel, the volume portion of austenite in the test piece was calculated according to formula [53-55]:

$$u_a = \frac{\frac{S_{IR\gamma}}{lp_\gamma}}{\frac{S_{IR_\gamma}}{lp_\gamma} + \frac{S_{IR_\alpha}}{lp_\alpha}} \cdot (100 - u_w)\%, \tag{1}$$

where:
lp_γ, lp_α - numbers of the analysed diffraction reflexes of γ and α phases,
u_w – volume portion of carbides or other intermetallic phases in steel (%),
$S_{IR\gamma}$, $S_{IR\alpha}$ - sums of quotients $\frac{I_\gamma}{R_\gamma}$, $\frac{I_\alpha}{R_\alpha}$ calculated according to formula:

$$S_{IR_\gamma} = \sum_{i=1}^{lp} \frac{I_{\gamma i}}{R_{\gamma i}}, \tag{2}$$

$$S_{IR_\alpha} = \sum_{i=1}^{lp} \frac{I_{\alpha i}}{R_{\alpha i}}, \tag{3}$$

where:
i – reflex number of γ and α phases,
lp – number of reflexes of γ and α phases,
$I_{\gamma i}$, $I_{\alpha i}$ – intensity of the i-th reflex of γ and α phases,
$R_{\gamma i}$, $R_{\alpha i}$ – coefficient R of the i-th reflex of γ and α phases, calculated according to formula:

$$R = \frac{1}{V^2} \cdot |Fhkl|^2 \cdot Lp \cdot Kp, \tag{4}$$

where:
V – volume of the elementary cell of γ and α phases,
$|Fhkl|$ - square of the amplitude value of the structure factor calculated according to formulae 5, 6,
Lp - polarization Lorentz factor,
Kp – multiplicity factor of the analyzed family of planes.

Amplitude of the structure factor for the face-centred cubic lattice (γ phases) and for the body-centred cubic lattice (α phase) is calculated according to formula:

$$Fhkl_\gamma = 4 f_a, \tag{5}$$

$$Fhkl_\alpha = 2 f_a, \tag{6}$$

where:
fa – X-ray radiation atomic scattering factor

Measurement results were taken into account in calculations of the X-ray radiation reflected from the lattice planes of γ and α phases, chemical compositions of these phases, as well as the portion of carbides undissolved during austenitization, and also conditions at which the experiment on the X-ray diffractometer was carried out.

Experimental results of the X-ray analysis were approximated using a combination of the base functions: one linear function (adjustment of the noise floor) and Voight function (matching the analysed Fe_γ and Fe_α reflexes, and MC carbides). Levenberg-Marquardt algorithm was used to determine the base functions parameters, in which the matching quality was characterized by χ^2 function value. The χ^2 function is defined as a sum of squares of the experimental distances results from values calculated from the determined mathematical model. The base functions parameters for which χ^2 function reaches its minimum indicate locations and intensities of reflexes on the diffraction pattern.

Separation of $Fe_\gamma(111)$ and $Fe_\alpha(011)$ reflexes intensities located in the range of angle 2θ about 50,5-53^o was done taking into account that also MC(200) reflex is in the analysed range (Figure 6). As the direct measurement of the MC(200) reflex intensity is impossible in the analysed test pieces, then it was assumed – according to data from the JCPDS index (card No 73-0476) – that intensity of this reflex is close to the MC(111) reflex intensity, located on the diffraction pattern at an angle $2\theta \approx 43{,}7^o$ [56]. Therefore, intensity corresponding to the $Fe_\gamma(111)$ reflex was defined by determining the total intensity of $Fe_\gamma(111)$ and MC(200) reflexes from which the value equal to the MC(111) reflex was subtracted next.

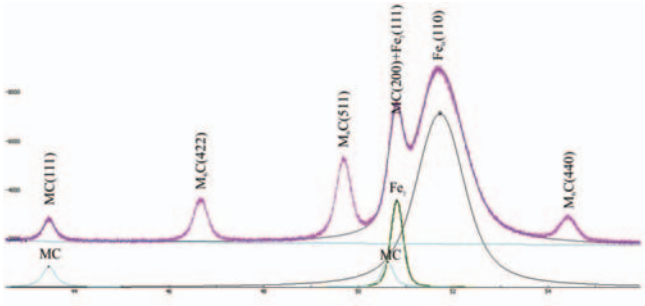

Fig. 6. Example of determining intensities of $Fe_\gamma(111)$, $Fe_\alpha(110)$ and MC(200) reflexes

Diffraction and thin foils structure examinations from the selected locations of the gradient high-speed steel matrix composites in the sintered state and heat treated were made on the JEOL JEM 3010UHR (TEM) transmission electron microscope at the accelerating voltage of 300 kV. The lamellae were mechanically thinned to thickness of about 80 μm on abrasive papers of 5-40 μm/mm^2 gradation using the Gatan thinning attachment, and next were subjected to final thinning on the Gatan ion polishing device. Thin foils prepared in this way were examined on the transmission electron microscope by structure observations in the bright and dark fields as well as diffraction examinations. The diffraction patterns from the transmission electron microscope were solved using the „Eldyf" computer program.

4.2. Examination of physical and mechanical properties

Specific weights (real) of the high-speed steel powders, WC and VC carbides were measured with the automatic Micromeritics AccuPyc 1330 gas pycnometer. Measurements were made in helium atmosphere. Bulk density of powders was calculated according to standard [57]. Flow rate of powders was determined according to standard [58].

Measurement of density, porosity, and hardness tested by Vickers and Rockwell in A scale methods were made on the sintered test pieces.

Densimetric method was used to measure density of the sintered test pieces, consisting in measurement of the apparent test piece mass when immersed in water [59].

Hardness testing with Vickers method was made at the indenter load of 4.903 N. Duration of the total indenter load was 15 s. The test was carried out on the entire transverse section width of the sintered test pieces, beginning from the distance of 0.2 mm from the external face of the surface layer up to the substrate layer zone (about four test points fell on each layer). Hardness tests with Rockwell in scale A were made on the end faces of the surface layers of the sintered gradient high-speed steel matrix composites. Tests were made at 10 locations selected randomly from the surface layers zones.

Stereological examinations were made to determine porosity using the Axiowert 405M optical microscope equipped with the computer image analysis system. Stereological examinations were made on microsections using the Image-Pro Plus computer image analysis system. Surface portion of pores was determined, as ratio of the pores area to the total area of the analysed region. Each time five random points from each layer were selected for tests.

Hardness tests with Rockwell in scale C were made on the end faces of the surface layers of the heat treated gradient high-speed steel matrix composites. For each heat treatment variant tests were made at randomly selected locations from the surface layers and substrate zones (10 measurements for each layer). Hardness tests were also made of the test pieces from the selected MG−75HSS/25WC material in the sintered state to compare the HRC hardness test results of materials before and after heat treatment.

Test results for density, porosity, and hardness were analysed statistically, calculating the arithmetic average, standard deviation, and confidence interval for each test series at the significance level α =0,05. The linear correlation coefficient was calculated for hardness and density measurement results of the sintered gradient high-speed steel matrix composites, and its test of significance was made.

Regression function was also determined approximating dependence of the investigated output variable Y (e.g., material hardness or its density) on the input variables X_i (e.g., volume portion of constituents, manufacturing process- or heat treatment conditions). Regression model used most often in the technological investigations was assumed in the form of [60,61]:

$$\hat{Y}(X) = \beta_0 + \sum_{i=1}^{L} \beta_i X_i + \sum_{i=1}^{L-1} \sum_{j=i+1}^{L} \beta_{ij} X_i X_j + \sum_{i=1}^{L} \beta_{ii} X_i^2, \quad \text{for } L \geq 2 \tag{7}$$

where:
$\hat{Y}(X)$ – regression function values for the input variables vector $X=[X_1X_2\ldots X_L]^T$,
$B_i\beta_{ij}$ – regression function coefficients determined with the least squares method,
L – number of input variables.

The regression function (7) has the following elements:

- constant - coefficient β_0,
- linear – first sum,
- interactions – double sum,
- square – last sum.

The full square model was developed for experiments in which the input variables assumed values at three variability levels at least, taking all components mentioned above into account. In other cases the model was developed taking interactions of variables into account, including a constant component, linear components, and interaction components.

Coefficients of the regression function were the results of the analysis, as well as intersections of function plots in planes defined by the selected values of the input variable, along with the confidence intervals for the forecasted value.

The multiple correlation coefficient was used as the regression function quality measure, expressing the level of its matching to the measurement results, defined by the formula [60,61]:

$$\hat{R}=\left(\frac{\sum_{j=1}^{M}(\hat{Y}(X_{ij})-\hat{Y})^2}{\sum_{j=1}^{M}(Y_j-\overline{Y})^2}\right)^{\frac{1}{2}}, \tag{8}$$

where:
$\hat{Y}(X_{ij})$ – regression function value for the input variables vector, corresponding to the j-th measurement,
$\overline{Y}$ – average of the output variable measurement results,
Y_j – result of the j-th output variable measurement.

Coefficient $\hat{R}$ assumes values in the range from 0 (when there is no correlation between two compared values) to 1 (if there is a functional relationship between the quantities).

Significance of the correlation coefficient, and therefore significance of the regression function significance, was determined by calculating the ratio

$$\hat{F}=\frac{(M-L)\hat{R}^2}{(L-1)(1-\hat{R}^2)}, \tag{9}$$

Correlation coefficient is significant at level α, if the $\hat{F}$ coefficient is bigger than the critical value of the F Fisher-Snedecor distribution for the particular significance level, and degrees of freedom of the numerator and denominator which are equal $(L-1)$ and $(M-L)$ respectively [62].

5. Description of achieved results while internal research

5.1. Test results of the sintered high-speed steel matrix composites

It was found out, based on observations of the sintered high-speed steel matrix composites structure, that increase of the WC tungsten- and VC vanadium carbides portions affect significantly the consolidation process. Structure of high-speed steel matrix composites with a low portion of the reinforcing phases, sintered both in the vacuum furnace and in the furnace with the flowing atmosphere of nitrogen with the addition of N_2+5%H_2 is characteristic of the high density and low inhomogeneity. The carbides undissolved in the high-speed steel matrix during sintering are fine and evenly distributed (Figure 7, 8). In case of the 90M2/10WC test pieces clusters of these carbides occur in vicinity of grain boundaries, which attests that the structural changes begin, connected with partial remelting of the grain boundaries (Figure 7 a, b).

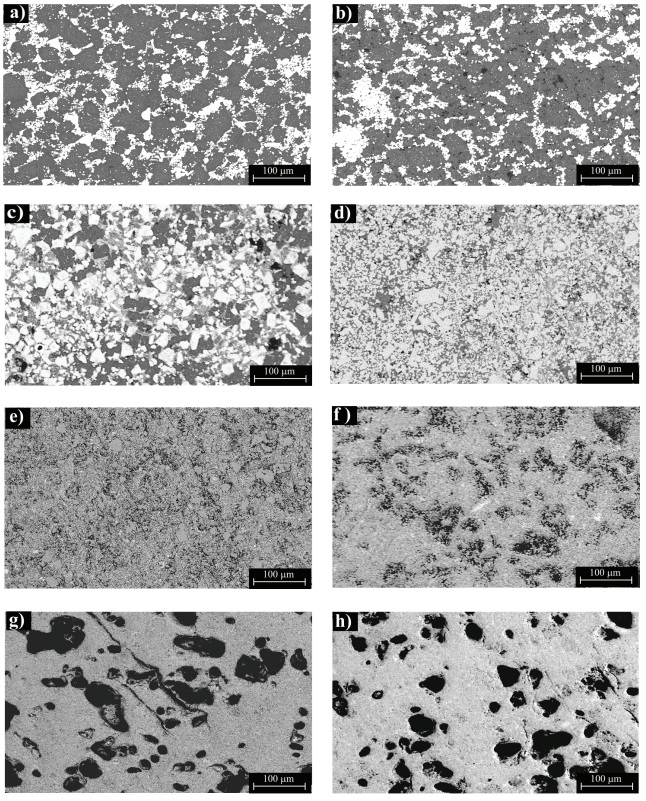

Fig. 7. Microstructures of high speed steel matrix composites reinforced with the WC tungsten carbide sintered at the temperature of 1250°C, for 60 min; in the vacuum furnace: a) 90HSS/10WC, c) 75HSS/25WC, e) 50HSS/50WC, g) 10HSS/90WC; in the atmosphere of the flowing N_2+5%H_2 gas mixture: b) 90HSS/10WC, d) 75HSS/25WC, f) 50HSS/50WC, h) 10HSS/90WC

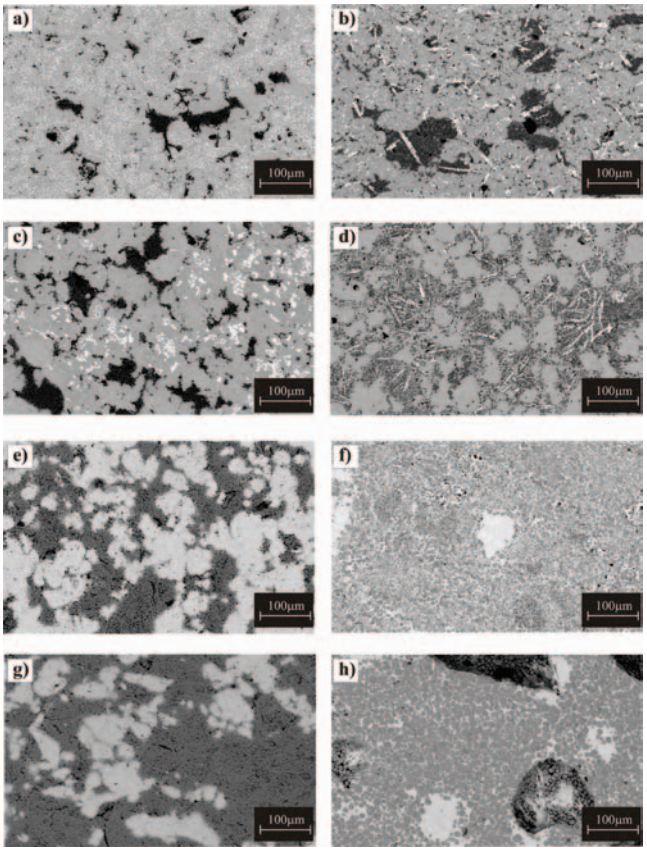

Fig. 8. Microstructures of high speed steel matrix composites reinforced with the VC vanadium carbide sintered at the temperature of 1250°C, for 60 min; in the vacuum furnace: a) 90HSS/10VC, c) 75HSS/25VC, e) 50HSS/50VC, g) 10HSS/90VC; in the atmosphere of the flowing N_2+5%H_2 gas mixture: b) 90HSS/10VC, d) 75HSS/25VC, f) 50HSS/50VC, h) 10HSS/90VC

In case of high-speed steel matrix composites reinforced with the vanadium carbide more inhomogeneous structure is observed than in case of high-speed steel matrix composites with the WC addition (Figure 8).

Concentration increase of the reinforcing phases to 25% in high-speed steel matrix composites results in the structure inhomogeneity growth (Figure 7 c, d, 8 c, d). Further increase of the WC or VC carbides results in the adverse structural changes (Figure 7 e-h, 8 e-h).

The test piece with the 75HSS/25WC composition melted during sintering (Figure 7 c, d). The temperature of 1250°C is too high for this composition. The test pieces were sintered in the same conditions, yet other test pieces with a lower (10%) and higher (50%, 75%) WC tungsten carbide portion did not melt. This may indicate that at this temperature the eutectic point occurs for such composition. The experiment was repeated many times and the same effect was always obtained.

A high portion of pores was observed in the structure of high-speed steel matrix composites reinforced with the WC tungsten carbide, sintered in the vacuum furnace and in the furnace with the atmosphere of flowing nitrogen with the addition of N_2+5%H_2, attesting to the incomplete sintering process (Figure 9). In the high-speed steel matrix composites reinforced with the VC vanadium carbide structure the surface portion of pores is decidedly smaller (Figure 10).

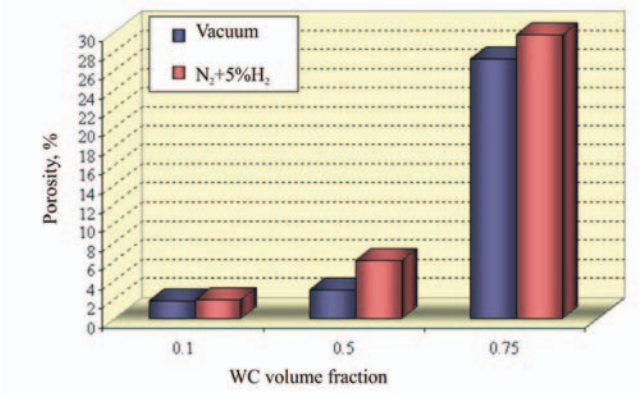

Fig. 9. Relationship between porosity and volume fraction of the reinforcing phase, for test pieces with the high-speed steel matrix composites reinforced with the WC tungsten carbide, sintered at the temperature of 1250°C, for 60 min; in the vacuum and in the atmosphere of the flowing N_2+5%H_2 furnace gas mixture

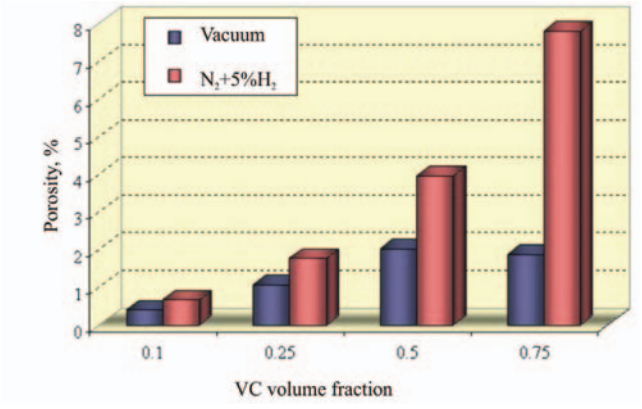

Fig. 10. Relationship between porosity and the volume fraction of the reinforcing phase, for test pieces with the high-speed steel matrix composites reinforced with the VC vanadium carbide, sintered at the temperature of 1250°C, for 60 min; in the vacuum and in the atmosphere of the flowing N2+5%H2 furnace gas mixture

Based on the X-ray microanalysis made with the EDX method in many micro-areas on the transverse sections of the test pieces significant differences of the chemical composition were observed in the selected analysis regions (Figures 11-13). In test pieces with the lower portion of the WC reinforcing phase these differences are especially distinct between the high-speed steel grains and carbides constituting agglomerations in the vicinity of grains boundaries. The lighter precipitations contain many carbide forming elements like W, Mo, V, and Cr. These are the MC type

carbides (light-grey precipitations) and the M_6C type carbides (white precipitations).

In the 90HSS/10WC test pieces sintered in the vacuum furnace vanadium concentration in the MC type carbides is ca. 34.8% at., other elements (W, Mo, Cr, and Fe) occur in these carbides in the significantly smaller concentrations (point 1 in Figure 11). In the M_6C type carbides Fe, C, and W dominate. Other elements, like Mo, Cr, and V occur in significantly smaller concentrations (point 2 in Figure 11). The remaining grey areas come from the matrix and contain mostly iron (point 3 in Figure 11).

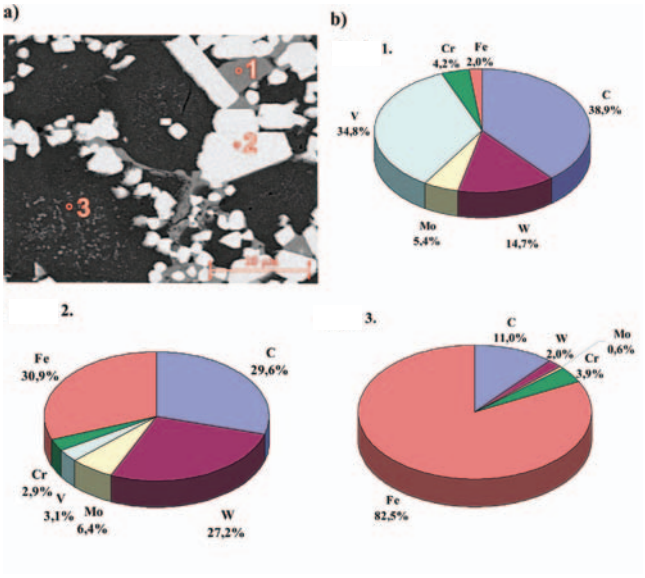

Fig. 11. SEM (BSE) micrograph a) of the high speed steel matrix composites with 25% content of WC, sintered at the temperature of 1250°C, for 60 min; in the vacuum furnace; b) EDAX analysis (%wt)

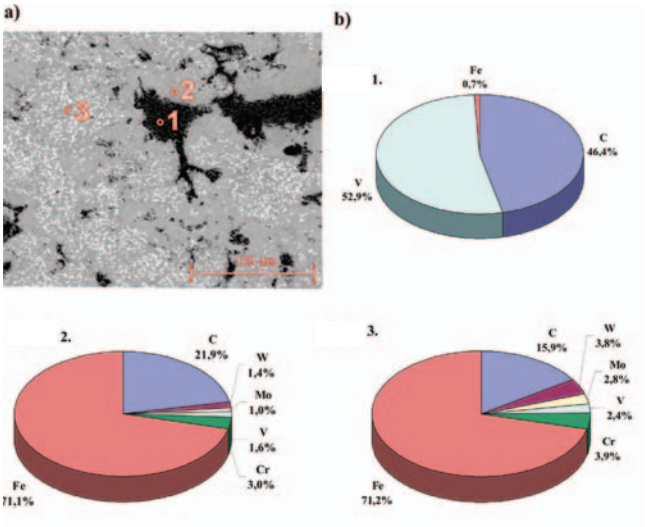

Fig. 12. SEM (BSE) micrograph a) of the high speed steel matrix composites with 10% content of VC, sintered at the temperature of 1250°C, for 60 min; in the vacuum furnace; b) EDAX analysis (%wt)

In the 90HSS/10VC, 75HSS/25VC test pieces the precipitations seen as the dark-grey areas are mainly V and C (point 1 in Figure 12 and point 2 in Figure 13). Grey areas are the matrix with the lighter precipitations containing C, W, Mo, V and Cr (point 2, 3 in Figure 12 and point 1 and 3 in Figure 13).

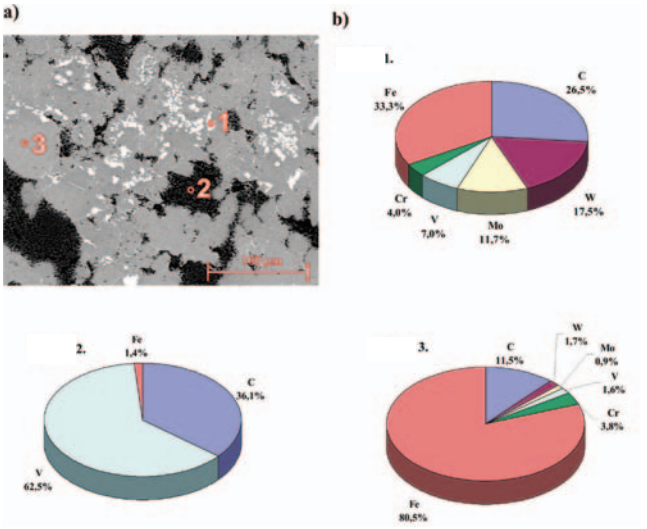

Fig. 13. SEM (BSE) micrograph a) of the high speed steel matrix composites with 25% content of VC, sintered at the temperature of 1250°C, for 60 min; in the vacuum furnace; b) EDAX analysis (%wt)

5.2. Test results of the gradient sintered high-speed steel matrix composites

The density measurement results obtained for the high-speed steel matrix composites reinforced with the VC vanadium carbide, sintered in the vacuum furnace and in the furnace with the atmosphere of the flowing nitrogen with the addition of hydrogen (N_2 + 5%H_2) are presented in Figures 14-19.

The density, of the compacted test pieces sintered in the vacuum furnace (Figures 14-16) and in the atmosphere of the flowing N_2-5%H_2 gas mixture (Figures 17-19), grows along with the sintering temperature increase. The highest density of test pieces with 10%VC and 25%VC was achieved for the sintering temperature 1270°C and sintering time 30 and 60 min., in the vacuum furnace. In case of the compacted test pieces sintered in the atmosphere (N_2-5%H_2), the highest density is different for the specimens with 10%VC and 25%VC. The density grows along with the sintering temperature increase and percentage volume portions of carbides. The highest density of test pieces with 10%VC was achieved for the sintering temperature 1270°C and sintering time 30 and 60 min, meanwhile for the 25%VC specimens the highest density was achieved for the sintering temperature 1250°C and sintering time 30 min, and for the sintering temperature 1230°C and sintering time 60 min.

The density measurement results obtained for the high-speed steel matrix composites reinforced with the WC tungsten carbide, sintered in the vacuum furnace and in the furnace with the atmosphere of the flowing nitrogen with the addition of hydrogen (N_2 + 5%H_2) are presented in Figures 20-25.

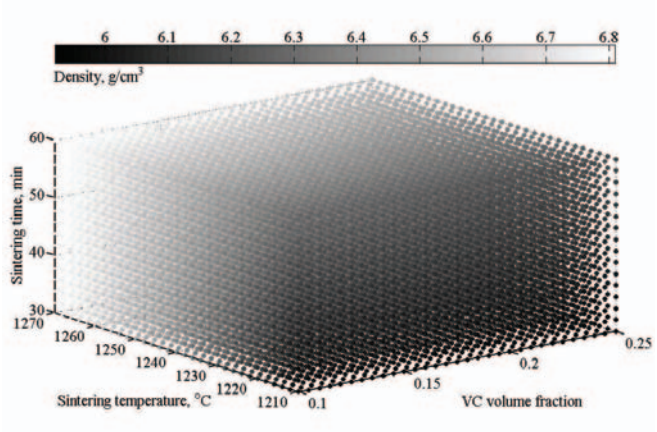

Fig. 14. Regression function plot describing relationship between density and the volume fraction of the reinforcing phase, temperature, and sintering time, for the gradient material reinforced with VC carbide, sintered in the vacuum furnace

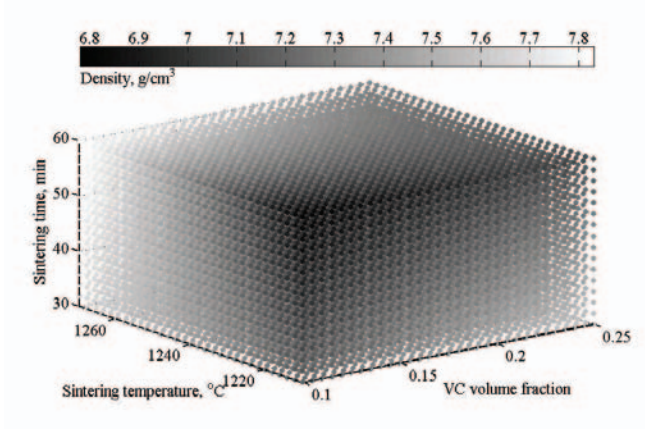

Fig. 17. Regression function plot describing relationship between density and the volume fraction of the reinforcing phase, temperature, and sintering time, for the gradient material reinforced with VC carbide, sintered in furnace with the atmosphere of the flowing nitrogen with addition of hydrogen (N_2+5%H_2)

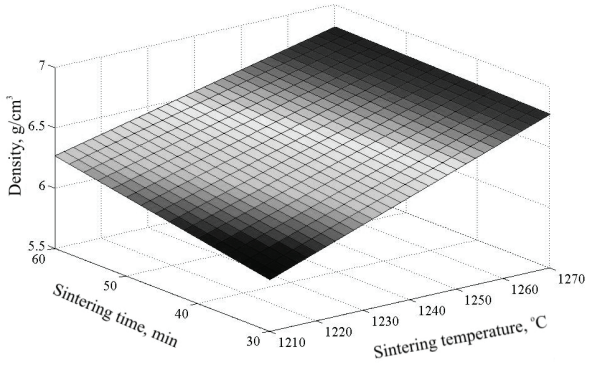

Fig. 15. Regression function plot describing relationship between density and the temperature, and sintering time, for the MG-90HSS/10VC material, sintered in the the vacuum furnace

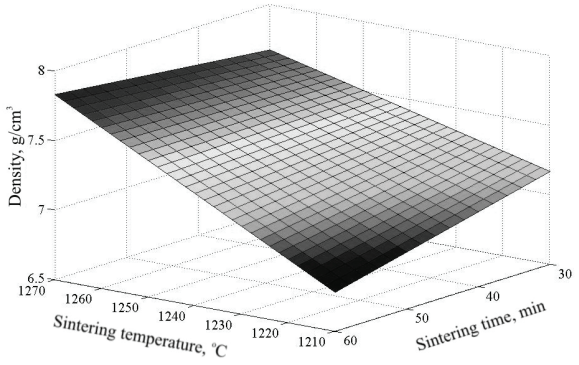

Fig. 18. Regression function plot describing relationship between density and the temperature, and sintering time, for the MG-90HSS/10VC material, sintered in furnace with the atmosphere of the flowing nitrogen with addition of hydrogen (N_2+5%H_2)

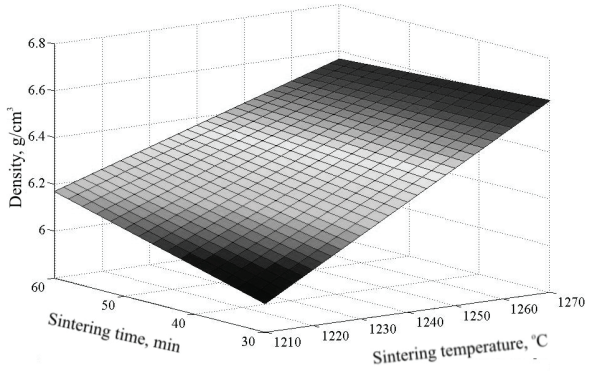

Fig. 16. Regression function plot describing relationship between density and the temperature, and sintering time, for the MG-75HSS/25VC material, sintered in the the vacuum furnace

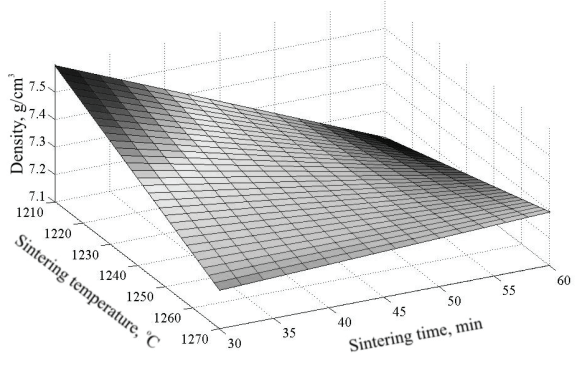

Fig. 19. Regression function plot describing relationship between density and the temperature, and sintering time, for the MG-75HSS/25VC material, sintered in furnace with the atmosphere of the flowing nitrogen with addition of hydrogen (N_2+5%H_2)

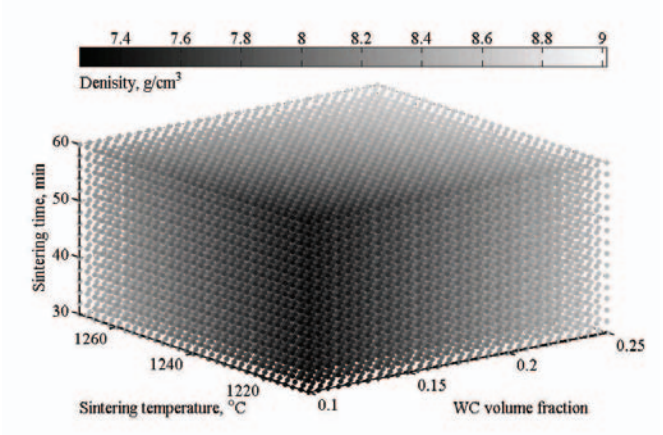

Fig. 20. Regression function plot describing relationship between density and the volume fraction of the reinforcing phase, temperature, and sintering time, for the gradient material reinforced with WC carbide, sintered in the vacuum furnace

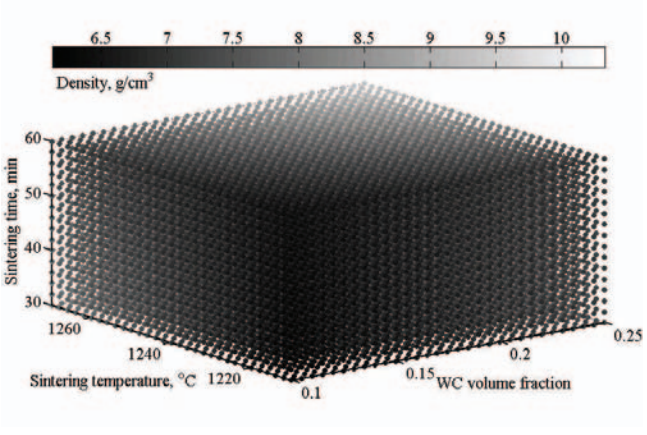

Fig. 23. Regression function plot describing relationship between density and the volume fraction of the reinforcing phase, temperature, and sintering time, for the gradient material reinforced with WC carbide, sintered in furnace with the atmosphere of the flowing nitrogen with addition of hydrogen (N_2+5%H_2)

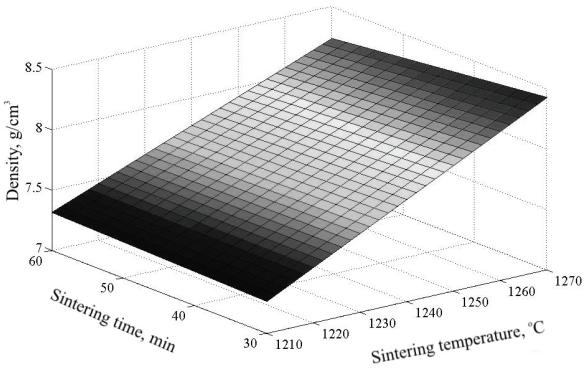

Fig. 21. Regression function plot describing relationship between density and the temperature, and sintering time, for the MG-90HSS/10WC material, sintered in the the vacuum furnace

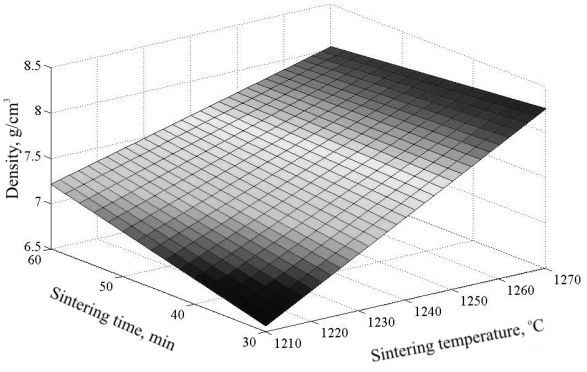

Fig. 24. Regression function plot describing relationship between density and the temperature, and sintering time, for the MG-90HSS/10WC material, sintered in furnace with the atmosphere of the flowing nitrogen with addition of hydrogen (N_2+5%H_2)

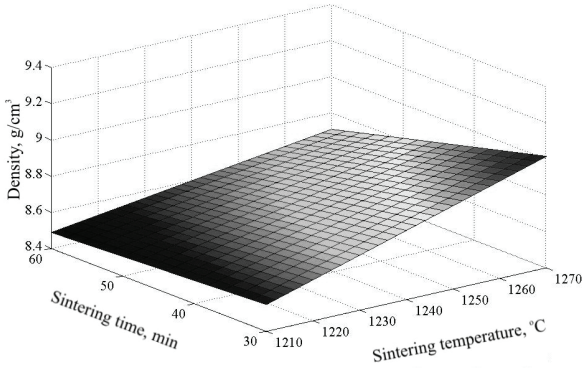

Fig. 22. Regression function plot describing relationship between density and the temperature, and sintering time, for the MG-75HSS/25WC material, sintered in the the vacuum furnace

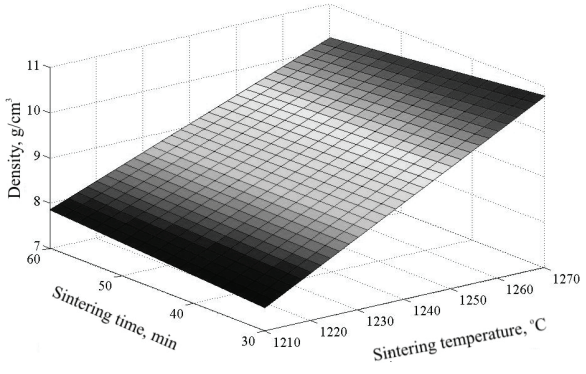

Fig. 25. Regression function plot describing relationship between density and the temperature, and sintering time, for the MG-75HSS/25WC material, sintered in furnace with the atmosphere of the flowing nitrogen with addition of hydrogen (N_2+5%H_2)

The highest density in case of the gradient cermets with the surface layer with the 90M2/10WC composition is ca. 8.22 g/cm^3). Extension of the sintering time to 60 minutes results also in a slight density growth (Figures 20-25). The maximum average density of ca. 8.49 g/cm^3 occurs in the test piece with the surface layer containing 75HSS/25WC after sintering at the temperature of 1230^{o}C. Density of the test piece with 10% tungsten carbide portion in its surface layer changes from ca. 6.42 g/cm^3 at the temperature of 1210^{o}C to maximum ca. 8.09 g/cm^3 at the sintering temperature of 1270^{o}C. Extension of the sintering time to 60 minutes does not result in a significant density growth.

The HRA hardness test results obtained for the face surfaces of the gradient high-speed steel matrix composites sintered in the vacuum furnace and in the furnace with the atmosphere of the flowing nitrogen with the addition of hydrogen (N_2+5%H_2) are presented in Figures 26-37.

It was found out based on hardness tests of the test pieces sintered in the vacuum furnace for 30 minutes (Figures 26-31) that in case of the test pieces with the 90HSS/10VC surface layer the lowest hardness of ca.44.6 HRA at the examined surface layer has the test piece sintered at the temperature of 1210^{o}C for 30 minutes. Increase of the sintering temperature to 1270^{o}C does not result in a significant hardness growth. The highest hardness of ca. 46.8 HRA was obtained for the test piece sintered at the temperature of 1250^{o}C. The average surface layer hardness with 10% portion of vanadium carbide changes slightly from ca. 43.2 HRA for T_s=1270^{o}C to maximum ca. 49.5 HRA for T_s=1250^{o}C.

Increase of the VC vanadium carbide concentration to 25% results in hardness decrease. Hardness of the surface layer with the 75HSS/25VC volume composition is characteristic of a lower hardness than the layer containing 90HSS/10VC after sintering in the same conditions, i.e., in the temperature range from 1210^{o}C to 1270^{o}C in steps of 20^{o}C for 30 minutes. The average hardness of the surface layer changes significantly as the sintering temperature increases in the range from ca. 28.8 HRA for T_s=1210^{o}C, to ca. 41.9 HRA, for T_s=1270^{o}C.

The average hardness of materials with an addition of the WC tungsten carbide in the HS6-5-2 high-speed steel is nearly four times higher in some cases than for materials with the addition of the VC vanadium carbide (Figures 29-31). The test piece with the surface layer of the 90HSS/10WC composition has the lowest average hardness at the temperature of 1210^{o}C – ca. 68.54 HRA. The average hardness grows with the sintering temperature increase to the value of ca. 80.5 HRA for the test piece sintered at the temperature of 1270^{o}C. Increase of WC concentration in the gradient material also results in hardness growth.

The average hardness for test pieces with the surface layer containing 25% WC, after sintering at the temperature of 1230^{o}C, is ca. 81.2 HRA for T_s=1210^{o}C and ca. 83.5 HRA. Extension of the sintering time to 60 minutes, in the same sintering conditions, in the temperature range from 1210 to 1270^{o}C does not cause big hardness changes of the investigated gradient high-speed steel matrix composites compared to hardness after sintering for 30 minutes. The maximum hardness of ca. 83.1 HRA occurs in the test piece with the surface layer containing 75HSS/25WC after sintering at the temperature of 1230^{o}C.

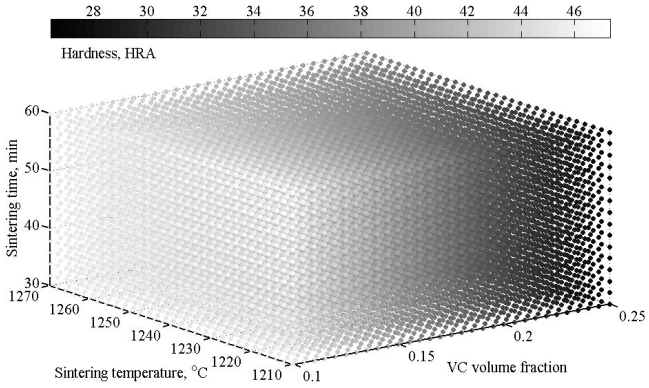

Fig. 26. Regression function plot describing relationship between hardness and the volume fraction of the reinforcing phase, temperature, and sintering time, for the gradient material reinforced with VC carbide, sintered in the vacuum furnace

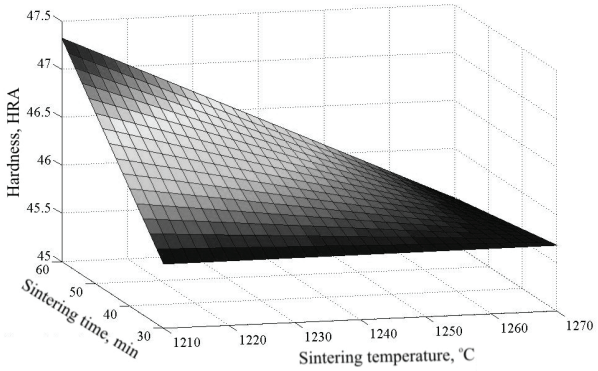

Fig. 27. Regression function plot describing relationship between hardness and the temperature, and sintering time, for the gradient material reinforced with 10% VC carbide, sintered in the vacuum furnace

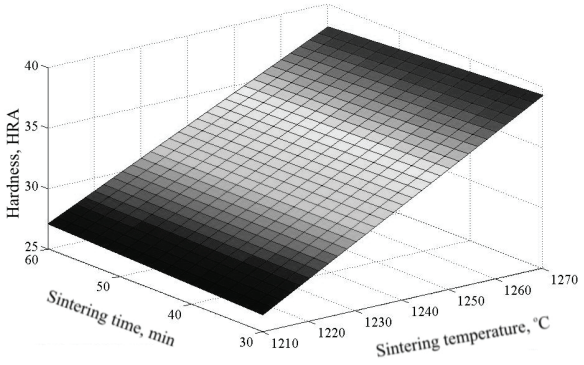

Fig. 28. Regression function plot describing relationship between hardness and the temperature, and sintering time, for the gradient material reinforced with 25% VC carbide, sintered in the vacuum furnace

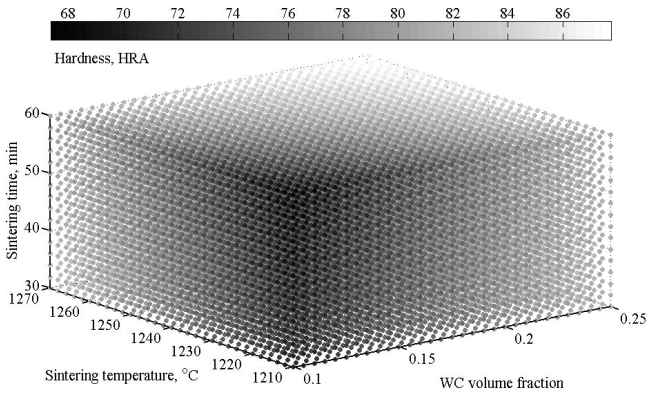

Fig. 29. Regression function plot describing relationship between hardness and the volume fraction of the reinforcing phase, temperature, and sintering time, for the gradient material reinforced with WC carbide, sintered in the vacuum furnace

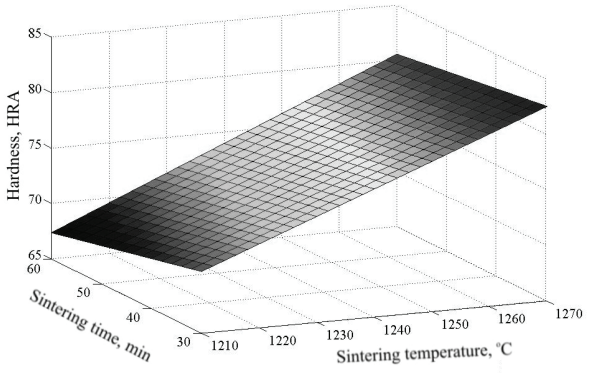

Fig. 30. Regression function plot describing relationship between hardness and the temperature, and sintering time, for the gradient material reinforced with 10% WC carbide, sintered in the vacuum furnace

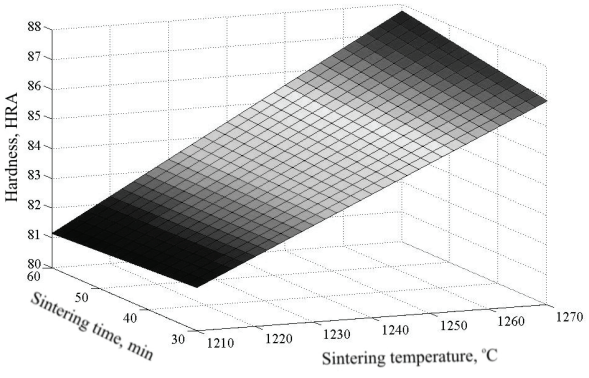

Fig. 31. Regression function plot describing relationship between hardness and the temperature, and sintering time, for the gradient material reinforced with 25% WC carbide, sintered in the vacuum furnace

It was found out, based on hardness tests of the test pieces sintered in the furnace with the atmosphere of the flowing nitrogen with the addition of nitrogen (N_2+5%H_2) for 30 minutes, that the test piece containing 10% of the VC vanadium carbide in its surface layer has the maximum hardness of ca. 76.5 HRA, after sintering at the temperature of 1250°C (Figures 32-34).

Increase of the VC vanadium carbide concentration to 25% does not cause hardness drop as it was the case with the test pieces with same chemical composition sintered in vacuum. No significant temperature effect was observed on average hardness of the test pieces with the surface layer with the 75HSS/25VC volume composition. The maximum average hardness in these test pieces is ca. 80.6 HRA after sintering at the temperature of 1230°C.

Extension of the sintering time to 60 minutes in the temperature range from 1210 to 1270°C causes in some cases hardness changes of the investigated gradient materials compared to hardness of the test pieces sintered for 30 minutes. The average value in case of the test pieces with the surface layer containing 90HSS/10VC varies from ca. 55.7 HRA for the test piece sintered at the temperature of 1210°C to ca. 75.1 HRA for the test piece sintered at the temperature of 1270°C. The maximum average hardness of ca. 79.4 HRA occurs for the test piece sintered at the temperature of 1250°C. Hardness grows with the VC vanadium carbide concentration increase to 25% in the surface layer, in the temperature range from 1210 to 1230°C. No substantial hardness growth was observed at a higher temperature along with the VC vanadium carbide concentration increase. The maximum average hardness for the test piece with the 90HSS/25VC surface layer is ca. 80.4 HRA for the test piece sintered at the temperature of 1250°C.

The significant effect of the sintering temperature on hardness is observed in the test pieces with the surface layer containing 90HSS/10WC. The minimum average hardness (ca. 56.7 HRA) was obtained for the test pieces sintered the temperature of 1210°C; whereas, the maximum one (ca. 80.6 HRA) for the test pieces sintered the temperature of 1270°C. After sintering in the same conditions hardness of the surface layer with a higher content of the WC tungsten carbide (25%) exceeds hardness of the 90HSS/10WC one. The maximum average hardness for this test piece is ca. 84.2 HRA after sintering at the temperature of 1230°C.

The sintering temperature increase affects substantially hardness of the test pieces containing 90HSS/10WC. The average hardness of the surface layer nearly doubles from ca. 43.2 HRA for the test piece sintered at the temperature of 1210°C to ca. 80.1 HRA for the test piece sintered at the temperature of 1270oC. The maximum hardness of ca. 84.2 HRA was obtained in the test pieces with the surface layer containing 75HSS/25WC for the test piece sintered at the temperature of 1230°C.

Structure photographs of the chosen four-layers gradient materials sintered in the vacuum furnace and in the furnace with the atmosphere of the flowing nitrogen with addition of hydrogen (N_2+5%H_2) taken on the scanning electron microscope are shown in Figures 38-41.

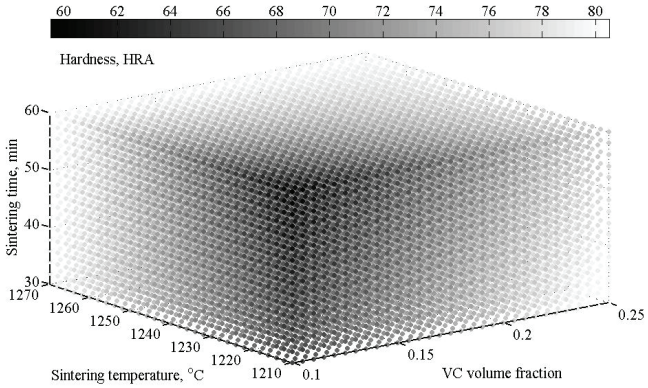

Fig. 32. Regression function plot describing relationship between hardness and the volume fraction of the reinforcing phase, temperature, and sintering time, for the gradient material reinforced with VC carbide, sintered in the furnace with the atmosphere of flowing nitrogen with addition of hydrogen (N_2+5% H_2)

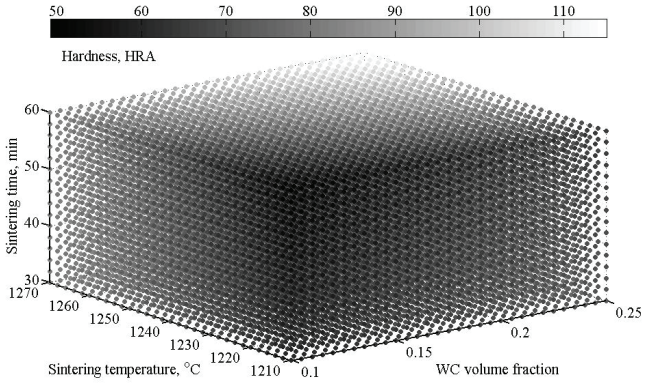

Fig. 35. Regression function plot describing relationship between hardness and the volume fraction of the reinforcing phase, temperature, and sintering time, for the gradient material reinforced with WC carbide, sintered in the furnace with the atmosphere of flowing nitrogen with addition of hydrogen (N_2+5% H_2)

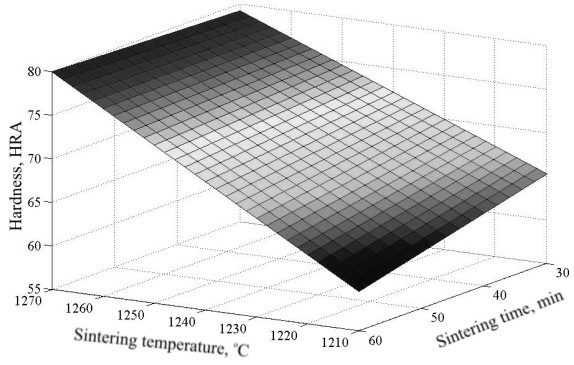

Fig. 33. Regression function plot describing relationship between hardness and temperature, and sintering time, for the gradient material reinforced with 10% VC carbide, sintered in the furnace with the atmosphere of flowing nitrogen with addition of hydrogen (N_2+5% H_2)

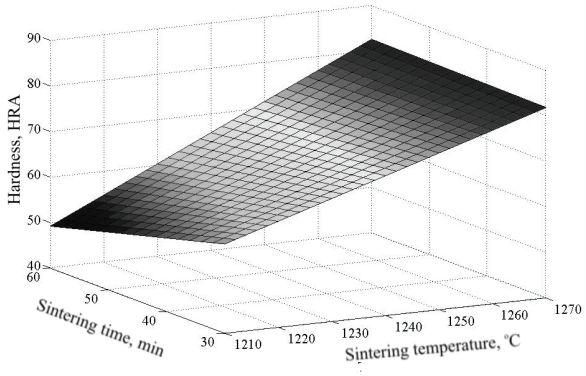

Fig. 36. Regression function plot describing relationship between hardness and the temperature, and sintering time, for the gradient material reinforced with 10% WC carbide, sintered in the furnace with the atmosphere of flowing nitrogen with addition of hydrogen (N_2+5% H_2)

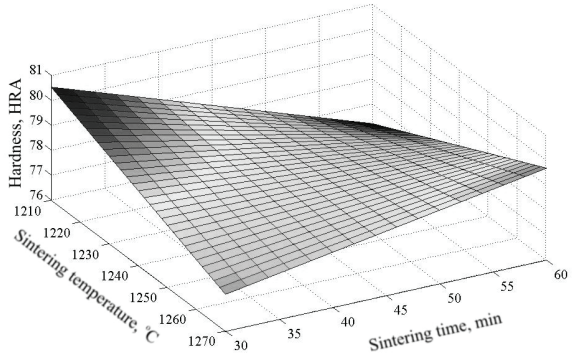

Fig. 34. Regression function plot describing relationship between hardness and temperature, and sintering time, for the gradient material reinforced with 25% VC carbide, sintered in the furnace with the atmosphere of flowing nitrogen with addition of hydrogen (N_2+5% H_2)

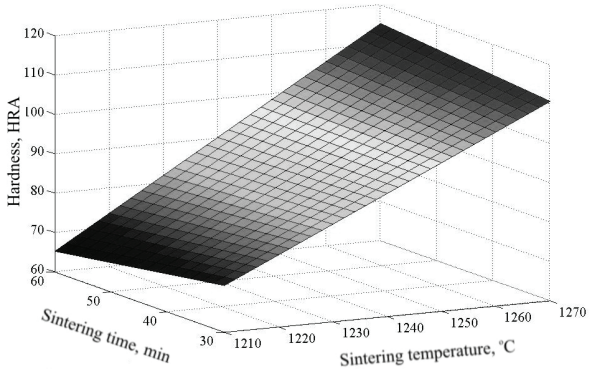

Fig. 37. Regression function plot describing relationship between hardness and the temperature, and sintering time, for the gradient material reinforced with 25% WC carbide, sintered in the furnace with the atmosphere of flowing nitrogen with addition of hydrogen (N_2+5% H_2)

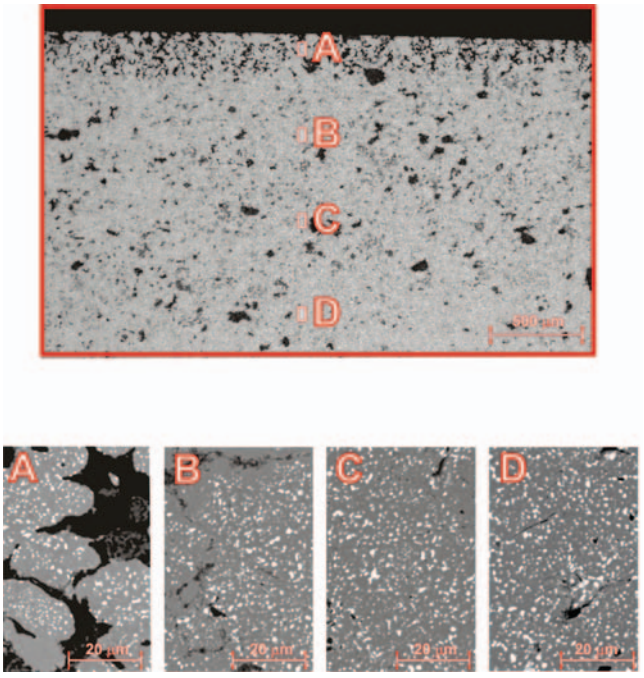

Fig. 38. Structure of layers of the MG-90HSS/10VC gradient material, sintered in vacuum furnace, at temperature *Ts* = 1210°C for *ts* = 30 min; composition of layers: A-HS6-5-2+10%VC, B-HS6-5-2+7%VC, C-HS6-5-2 +4%VC, D-HS6-5-2

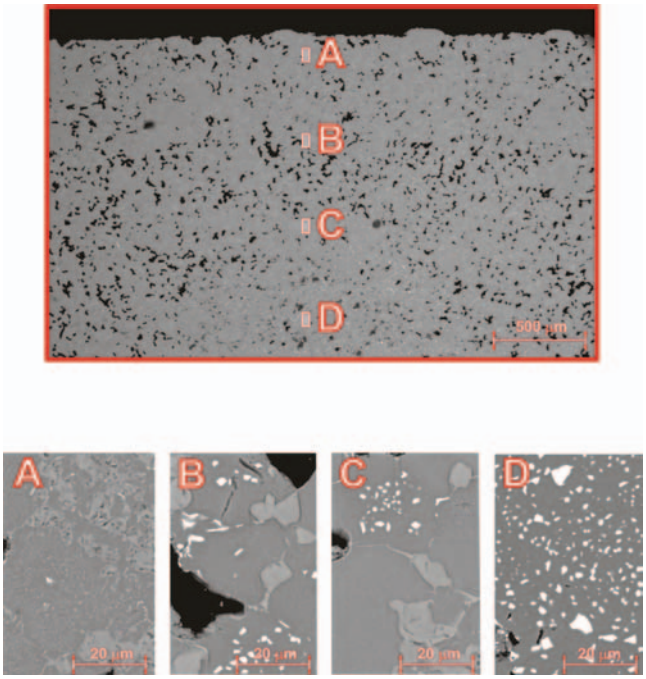

Fig. 39. Structure of layers of the MG-90HSS/10VC gradient material, sintered in vacuum furnace, at temperature *Ts* = 1270°C for *ts* = 60 min; composition of layers: A-HS6-5-2+10%VC, B-HS6-5-2+7%VC, C-HS6-5-2 +4%VC, D-HS6-5-2

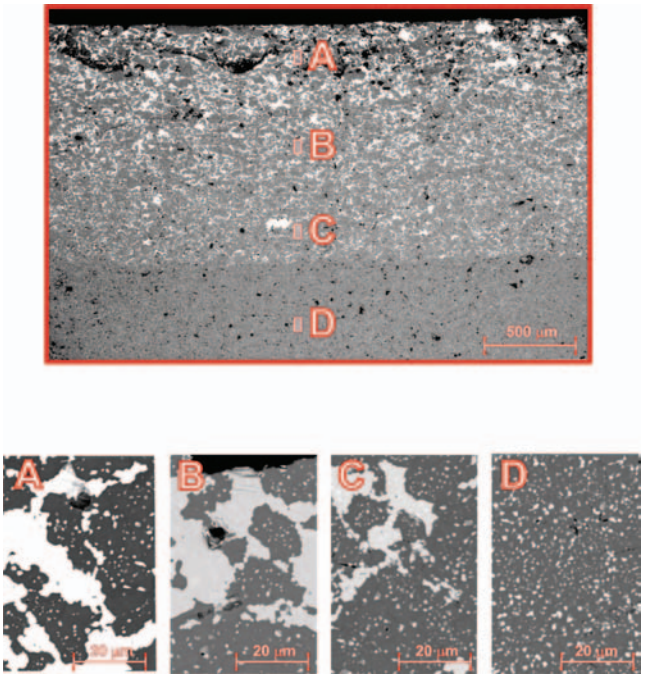

Fig. 40. Structure of layers of the MG-90HSS/10WC gradient material, sintered in vacuum furnace, at temperature *Ts* = 1210°C for *ts* = 30 min; composition of layers A-HS6-5-2+10%WC, B-HS6-5-2+7%WC, C-HS6-5-2 +4%WC, D-HS6-5-2

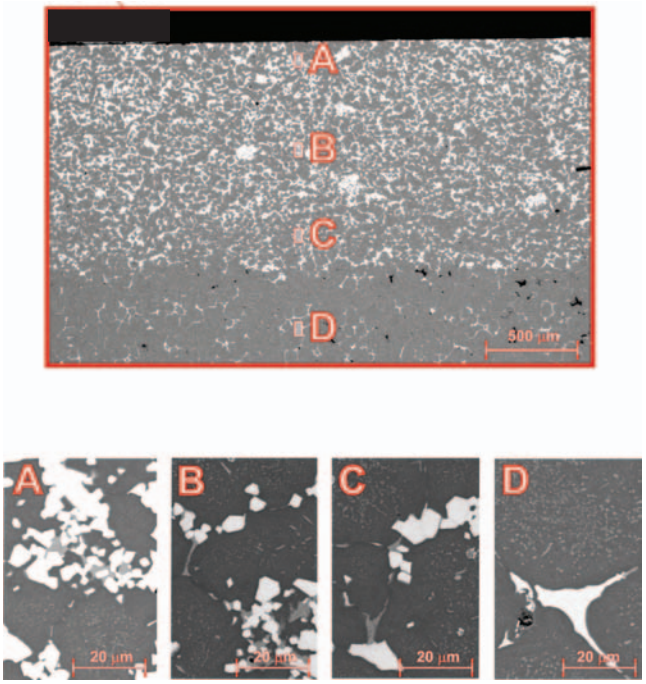

Fig. 41. Structure of layers of the MG-90HSS/10WC gradient material, sintered in vacuum furnace, at temperature *Ts* = 1270°C for *ts* = 60 min; composition of layers A-HS6-5-2+10%WC, B-HS6-5-2+7%WC, C-HS6-5-2 +4%WC, D-HS6-5-2

The highest portion of the transverse section area with the increased porosity is characteristic of the high-speed steel matrix composites reinforced with the VC vanadium carbide, sintered at the temperature 1210°C for 30 min. The increased porosity area spreads in the surface layers (Figures 42-43). A higher portion of pores is observed in peripheries of the test pieces sintered in the vacuum furnace for T_s=30 min with the 90HSS/10VC compositions (Figure 38). One can also see that the vanadium carbides occupy big areas close to pores. Boundaries between layers are barely discernible. Portion of pores decreases in the transition zone between the surface layer and the internal one. Increase of the sintering temperature to 1270°C results in porosity decrease in all test pieces.

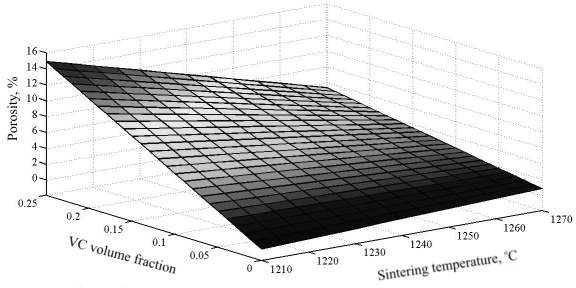

Fig. 42. Regression function plot describing relationship between porosity and the volume fraction of the reinforcing phase and sintering temperature, for the high-speed steel matrix composites reinforced with the VC vanadium carbide, sintered in the furnace with the atmosphere of flowing nitrogen with addition of hydrogen (N_2+5% H_2)

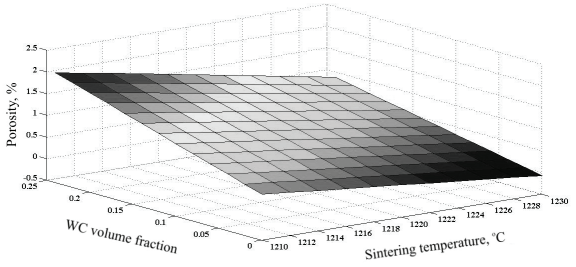

Fig. 43. Regression function plot describing relationship between porosity and the volume fraction of the reinforcing phase and sintering temperature, for the high-speed steel matrix composites reinforced with the WC tungsten carbide, sintered in the vacuum furnace for 30 min

The effect of temperature and sintering time on structure of the surface layers containing WC or VC and layers with the high-speed steel alone is shown in Figures 44-47.

No meaningful changes in structure were noticed in substrate layers containing the high-speed steel alone for the gradient high-speed steel matrix composites with the 90HSS/10VC, surface layers, sintered at temperatures of Tsp =1210, 1230, 1250, 1270°C for 30 and 60 minutes. The MC type carbides are fine and evenly distributed. The carbides are slightly bigger only for the test piece sintered at the temperature of 1270°C and time of 60 minutes (Figures 44, 45).

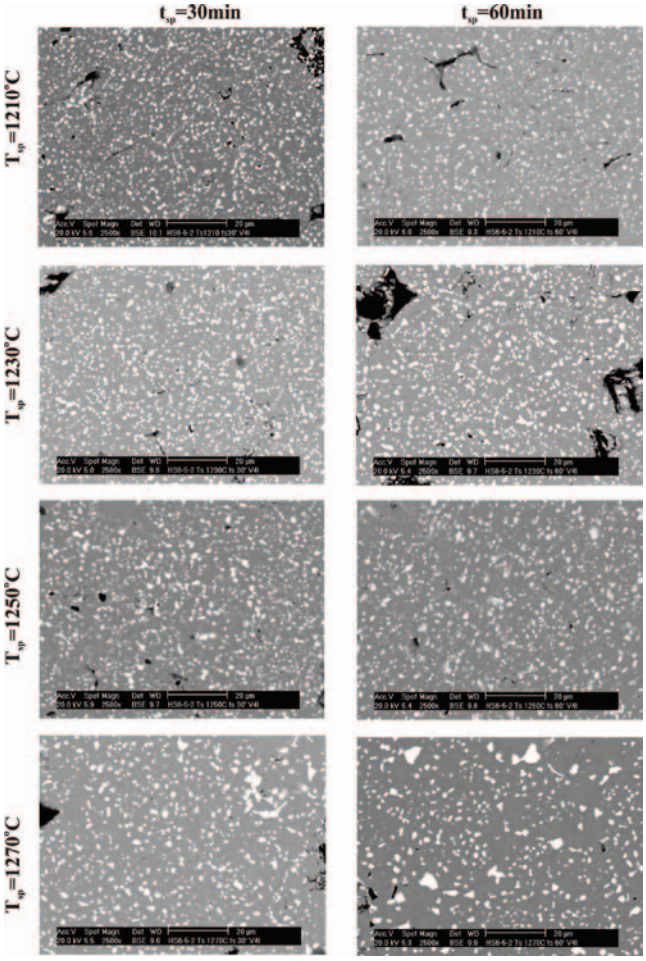

Fig. 44. Structure of the high-speed steel layer of the MG-90HSS/10VC material, sintered in vacuum furnace at temperatures of 1210, 1230, 1250, 1270°C for 30 and 60 min

Effect of temperature and time is essential in materials containing tungsten carbides. Structure change of the layer with the high-speed steel is discernible for the test piece sintered at the temperature of 1230°C and time of 60 min in test pieces with the 90HSS/10WC surface layer (Figure 45). Some carbides occupy areas with the concave surfaces and have the shape characteristic of the eutectic ones. These areas originated from the liquid state and crystallised as the last ones, among the austenite grains. Temperature increase causes growth and coagulation of the primary carbides. The structure appears characteristic of the remelted high-speed steel. Big carbides are distributed mostly at grain boundaries; whereas, the fine carbides are distributed inside the grains. More and more areas with the eutectic carbides are observed upwards from the temperature of 1250°C and time of 60 minutes. For T_s=1270°C only the elongated narrow carbides are observed distributed at some grain boundaries. The similar structure occurs also in materials with the 75HSS/25WC surface layer (Figure 46).

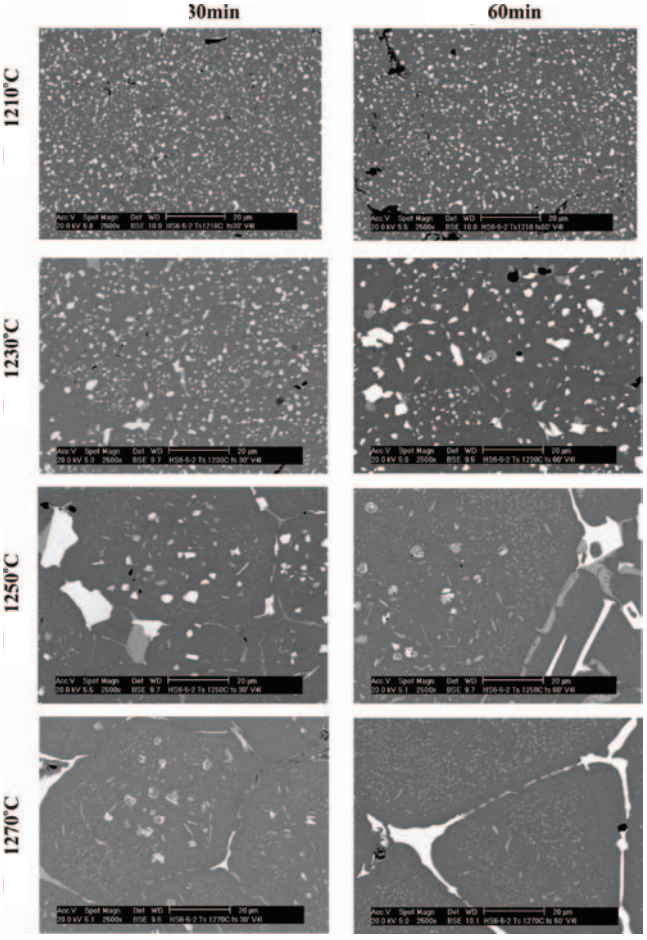

Fig. 45. Structure of the high-speed steel layer of the MG-90HSS/10WC material, sintered in vacuum furnace at temperatures of 1210, 1230, 1250, 1270°C for 30 and 60 min

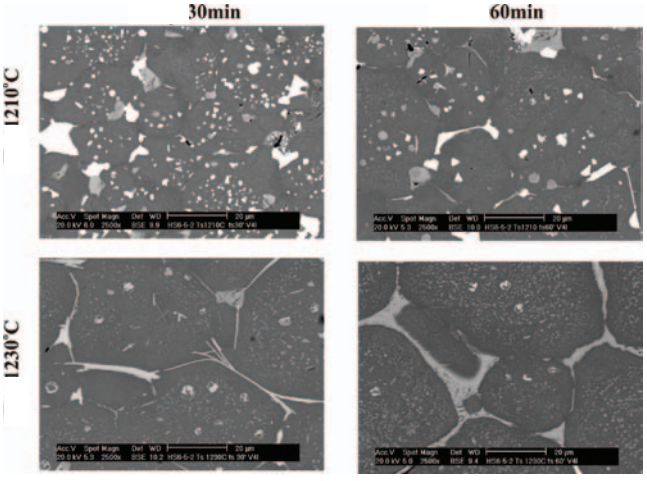

Fig. 46. Structure of the high-speed steel layer of the MG-75HSS/25WC material, sintered in vacuum furnace at temperatures of 1210, 1230, 1250, 1270°C for 30 and 60 min

Effect of the sintering temperature and time is essential in test pieces with the surface layer containing the vanadium carbide (Figure 47). The portion of pores, visible as black areas in the back-scattered electrons image, gets lower along with the sintering temperature and time.

Big agglomerations of the tungsten carbides, visible as light areas, occur in the surface layers of materials with the WC tungsten carbide. Eutectic carbides occur only at sintering at the temperature T_s=1250°C and time T_s=30 min (Figure 48). Concentration increase of the tungsten carbides to 25% results in growth of these carbides (Figure 49).

Test piece with the 75HSS/25WC volume composition of the surface layer was selected based on the microstructure observations. The green compact photograph is shown in the figure 50 as well as its fracture with four layers with the changing WC reinforcing phase portions. The most discernible boundaries are those between the layer from the high-speed steel and the layer with 5% addition of the tungsten carbide. These boundaries vanish along with the WC concentration increase.

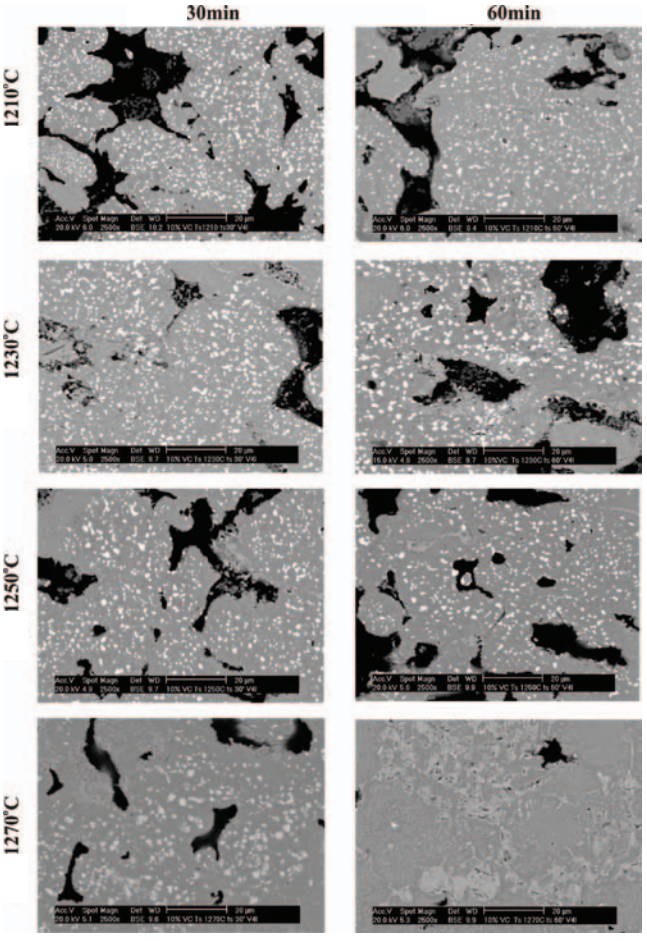

Fig. 47. Structure of the surface layer of the MG-90HSS/10VC material, sintered in vacuum furnace at temperatures of 1210, 1230, 1250, 1270°C for 30 and 60 min

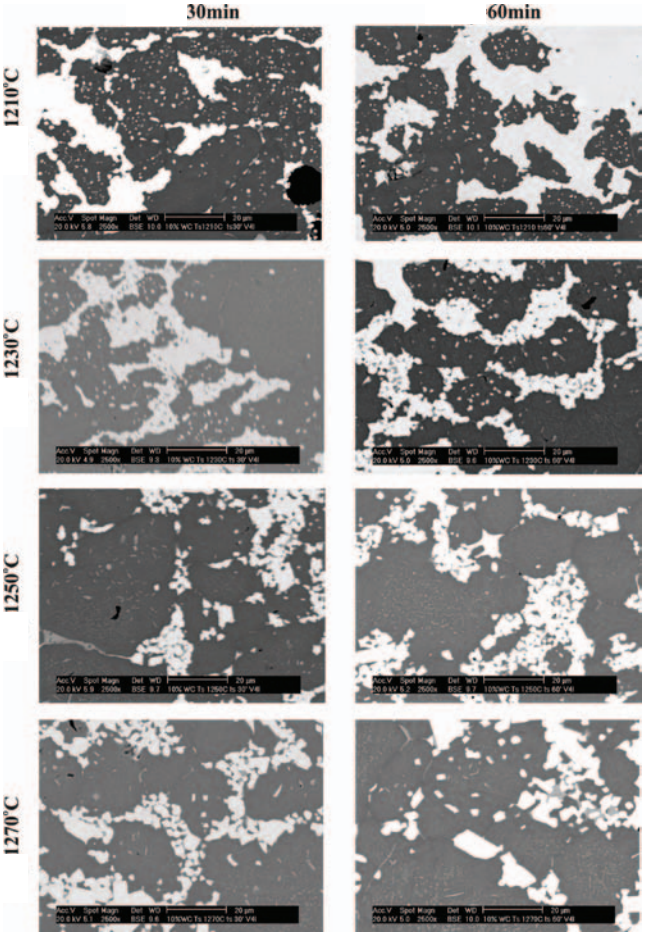

Fig. 48. Structure of the surface layer of the MG-90HSS/10WC material, sintered in vacuum furnace at temperatures of 1210, 1230, 1250, 1270°C for 30 and 60 min

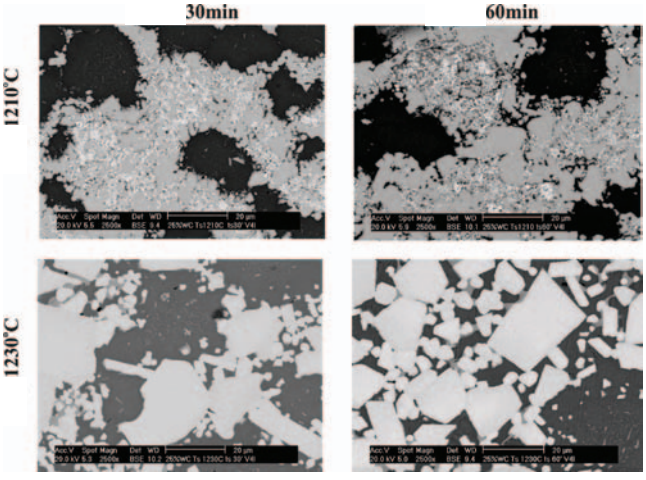

Fig. 49. Structure of the surface layer of the MG-75HSS/25WC material, sintered in vacuum furnace at temperatures of 1210, 1230, 1250, 1270°C for 30 and 60 min

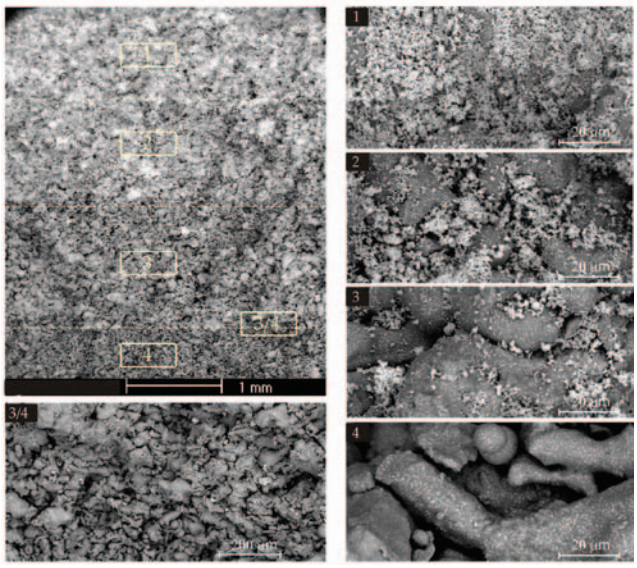

Fig. 50. The green compact photograph as well as its fracture with four layers with changing WC reinforcing phase portions

It was found out, based on the X-ray diffraction analysis, that the 75HSS/25WC material structure is composed of ferrite, inclusions of tungsten carbide and the MC and M_6C carbides. The new W_2C phase appears in the material due to sintering, the one that does not occur in the structures of the high-speed steel powder or in the sintered high-speed steel (Figure 51). Origination of this phase in the material structure is the effect of the chemical reaction between the high-speed steel and the WC tungsten carbide probably. These results were confirmed during the thin foils examinations (Figure 52).

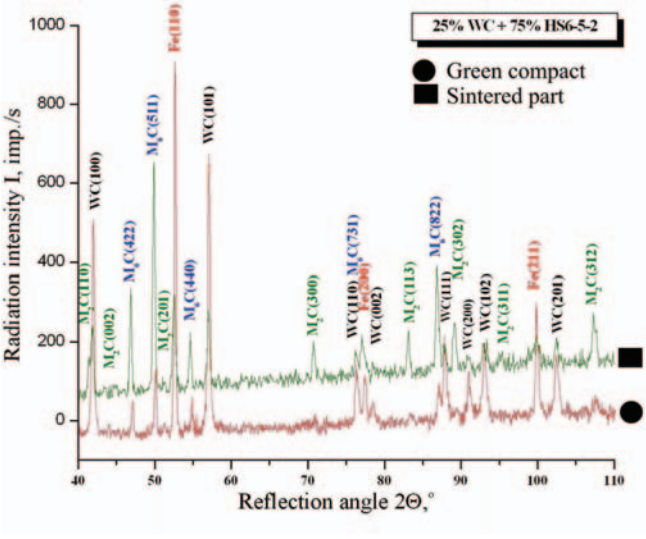

Fig. 51. Results of the X-ray phase analysis for the sintered test piece with the 75HSS/25WC surface layer; diffraction patterns were shifted along the vertical axis to show the results more clearly

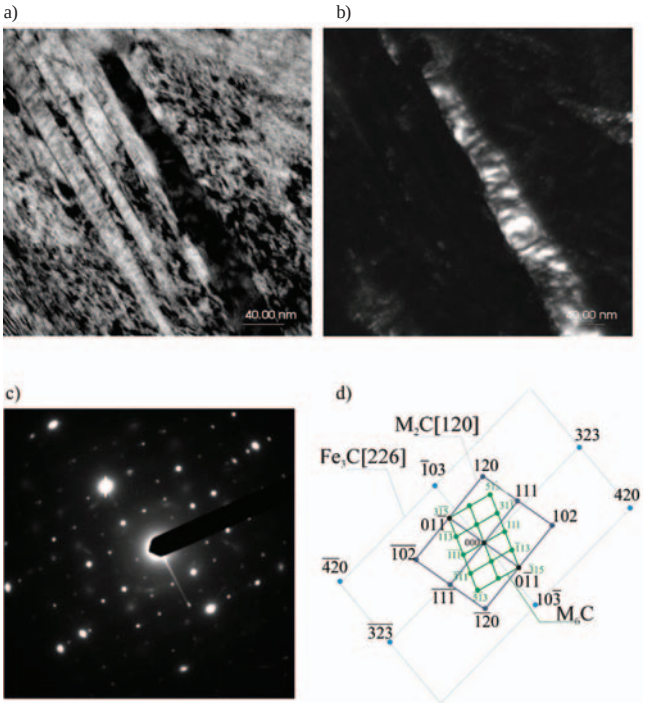

Fig. 52. Structure of thin foil from the surface layer of the MG-75HSS/25WC material, sintered in a vacuum furnace at temperature of 1250°C for 60 min; a) image in the bright field, b) image in the dark field, c) diffraction pattern from the area as in Figure a, d) solution of the diffraction pattern from Figure c

5.3. Heat treatment conditions

Regression function plots describing dependence of hardness on austenitizing temperature (T_a), austenitizing time (t_a), and second tempering temperature ($T_t II$) and their transverse sections in planes specified by the selected input variables along with the confidence intervals at the level of α=0.05 are shown in Figures 53-55 for the substrate layers and in Figures 56-58 for the surface layer.

It was shown based on the regression function variability analysis that the effect of heat treatment conditions, in the range assumed in the project, on hardness of the investigated gradient materials in the hardened and tempered state is observable solely in the substrate layers from the high-speed steel only (Figure 53-55). Hardness tests of the substrate layers of the gradient cermets in the heat treated state demonstrate clear effect of the tempering temperature on hardness value. The maximum secondary hardness effect of about 66.7 HRC was obtained in the gradient cermets austenitized at the temperature of 1210°C for 80 s, hardened and tempered at the temperature of 560°C. Increasing the tempering temperature to 590°C results in hardness drop compared to the conditions corresponding to the secondary hardness effect by about 1 HRC – in case of materials austenitized at the temperatures of 1180 and 1210°C and by about 2 HRC – for materials austenitized at the temperature of 1150°C. The biggest hardness drop after tempering in the analogous conditions by about 3 HRC was revealed in the substrate layers of the gradient materials previously hardened at the temperature of 1120°C. Hardness of the surface layer of gradient cermets is within the 69.2-71.6 HRC range.

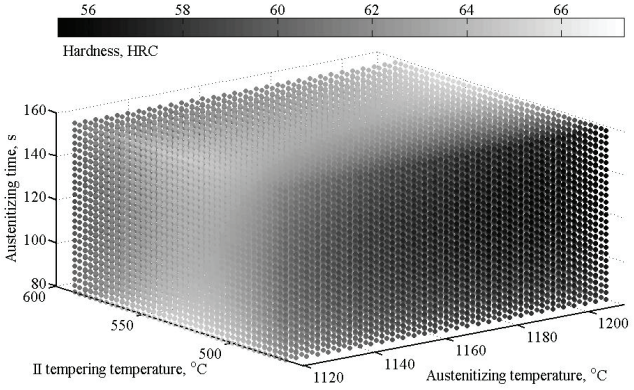

Fig. 53. Regression function plot describing relationship between hardness and the temperature, and austenitizing time, and second tempering temperature for the substrate layer (100% HSS) of the MG-75HSS/25WC

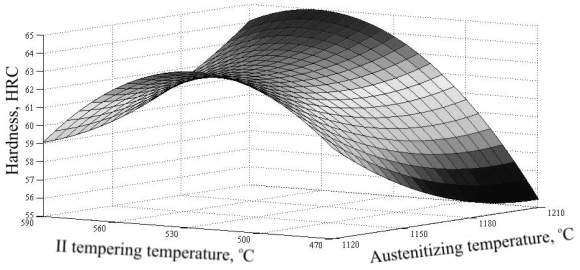

Fig. 54. Regression function plot describing relationship between hardness and the second tempering temperature, and the austenitizing temperature, for the substrate layer (100% HSS) of the MG-75HSS/25WC material austenitized for 120 s

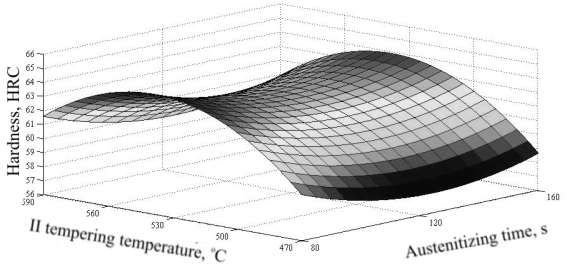

Fig. 55. Regression function plot describing relationship between hardness and the second tempering temperature, and the austenitizing time, for the substrate layer (100% HSS) of the MG-75HSS/25WC material austenitized at the temperature of 1150°C

Carrying out heat treatment in conditions used in the project results in the significant hardness increase in the surface layer of the gradient cermets by 5.8 - 8.2 HRC up to the values in the 69.2-71.6 HRC range (Figure 56). The highest surface layer hardness of 71.6

HRC is characteristic of the material austenitized at the temperature of 1120°C for 120 s, hardened, and next tempered twice at the temperature of 530°C. No statistically significant effect was found of the heat treatment conditions change in the investigated range on the surface layers hardness after hardening and tempering of the gradient materials containing 25% WC.

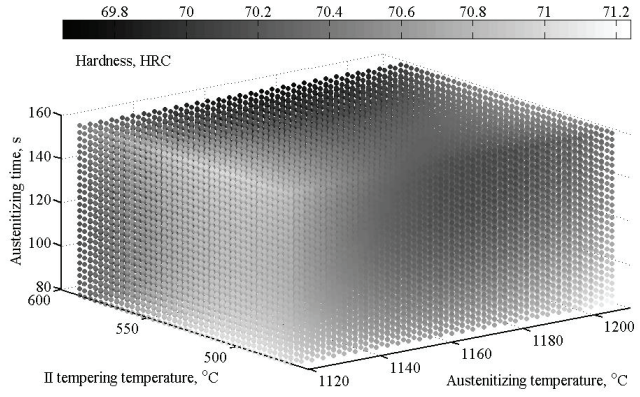

Fig. 56. Regression function plot describing relationship between hardness and the temperature, and austenitizing time, and second tempering temperature for the surface layer (75%HSS+25%WC) of the MG-75HSS/25WC

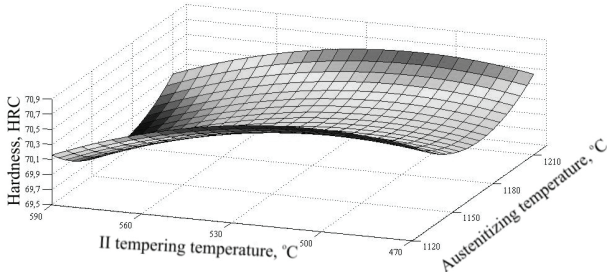

Fig. 57. Regression function plot describing relationship between hardness and the second tempering temperature, and the austenitizing time, for the surface layer (75%HSS+25%WC) of the MG-75HSS/25WC material austenitized for 120 s

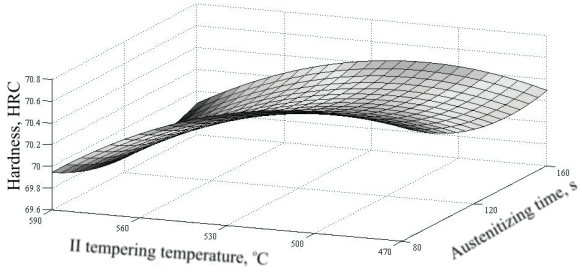

Fig. 58. Regression function plot describing relationship between hardness and the second tempering temperature, and austenitizing time, for the surface layer (75%HSS+25%WC) of the MG-75HSS/25WC material austenitized at the temperature of 1150°C

Structure of the investigated gradient cermets in the hardened state is martensite with the retained austenite, M_6C and MC type carbides, primary, and also secondary ones, undissolved in the solid solution during austenitizing, as well as the WC tungsten carbides in the surface layer of the materials, which was confirmed with the X-ray phase analysis method (Figure 59). The M_6C and MC type carbides undissolved in the solid solution during austenitizing were idenfied also with the electron diffraction method and observed using the dark field during examinations of the thin foils on the transmission electron microscope (Figure 60).

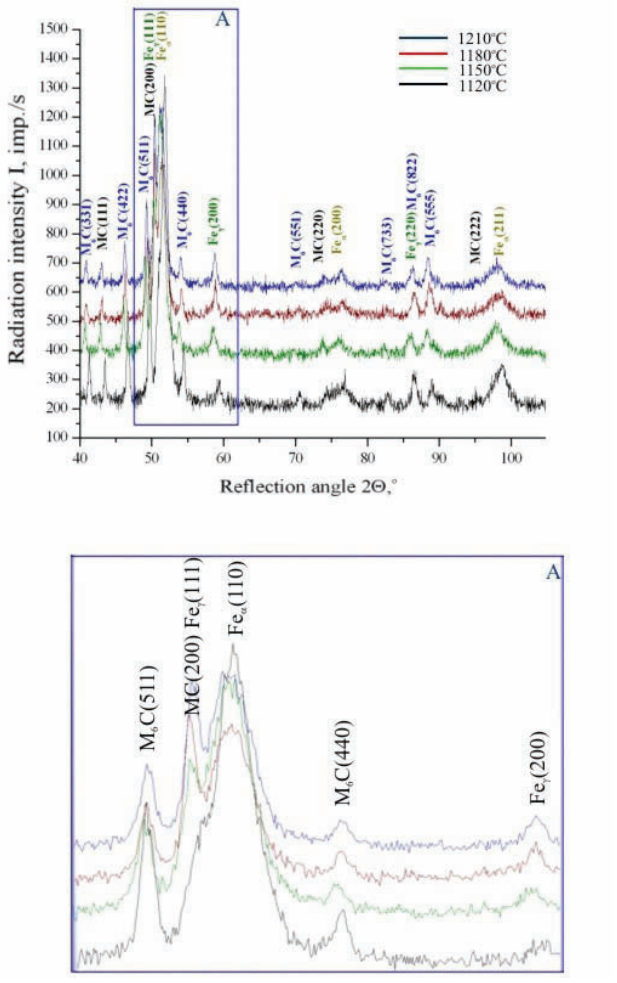

Fig. 59. Results of the X-ray phase analysis from the substrate layer (100% HSS) of the MG-75HSS/25WC test piece, austenitized at temperature of 1210°C for 120 s; diffraction patterns were shifted in respect to the vertical axis to show the results more clearly

The primary and secondary carbides, undissolved in the solid solution during austenitizing, affect significantly the primary austenite grain size. Figure 61 present the surface portion analysis results for the carbides, calculated with the quantitative metallography methods. Changes of the primary austenite grain size coefficient according to Snyder-Graff in the substrate layers containing 100% of the HS6-5-2 high-speed steel of the gradient

materials, versus temperature and austenitizing time are presented in Figure 62. The substrate layer of the gradient cermet hardened at the temperature of 1120°C and austenitized for 80 s demonstrates the primary grain size of the Snyder-Graff coefficient value of about 12. The primary austenite grain size grows along with the increase of the austenitizing temperature, reaching the Snyder-Graff coefficient value of about 6 after hardening at the temperature of 1210°C. Extending the austenitizing time fosters also growth of the primary austenite grain, whereas, extension of the austenitizing time affects it less than increasing the austenitizing temperature.

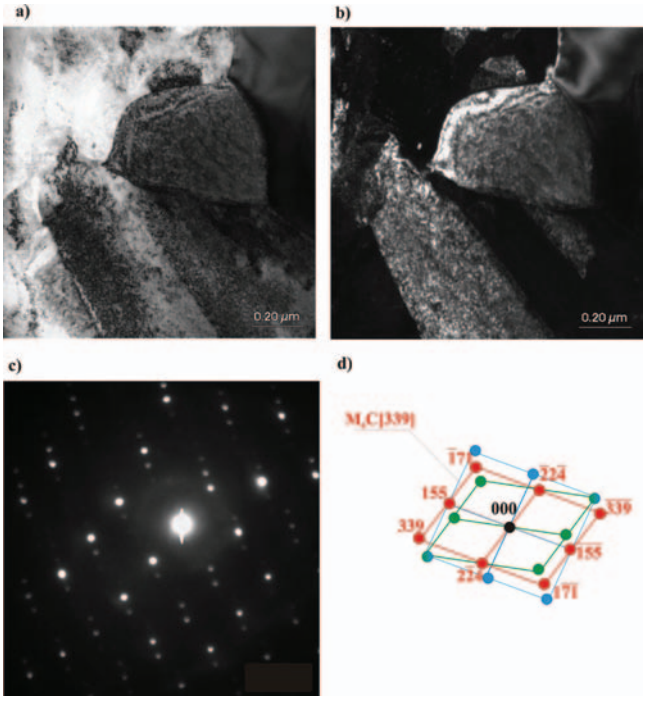

Fig. 60. Structure of thin foil from the surface layer of the MG-75HSS/25WC material, austenitized at temperature of 1150°C for 80 s; a) image in the bright field, b) image in the dark field, c) diffraction pattern from the area as in Figure a, d) solution of the diffraction pattern from Figure c

The substrate of the investigated gradient cermets in the state hardened at the temperature of 1210°C, which ensures the maximum secondary hardness after tempering, features the martensite with the retained austenite. The volume portion of the retained austenite in the structure of the investigated substrate layers of the hardened gradient cermets depends on the austenitizing conditions. It was found out with the X-ray quantitative phase analysis method that the volume portion of the retained austenite of the hardened test pieces ranges from about 5.7 to 26.5 % (Figure 63).

The volume portion of the retained austenite in the substrate layer of the gradient cermets hardened at the temperature of 1210°C, ensuring the maximum secondary hardness after its subsequent tempering at the temperature range from 470 to 590°C gets smaller depending on the second tempering temperature and is within the range from 1.6-23.8% respectively (Figure 64).

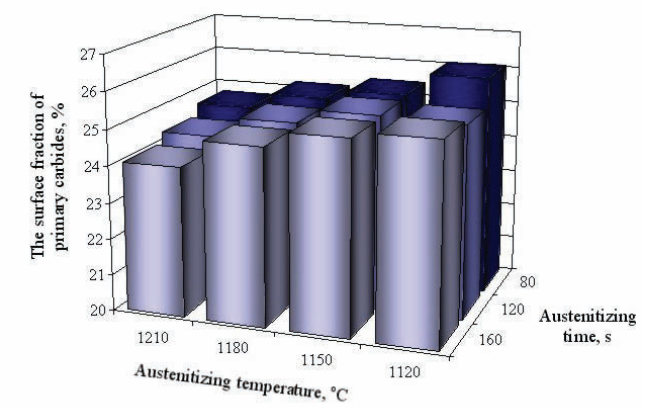

Fig. 61. Relationship between the surface portion of carbides in the substrate layer of the hardened high-speed steel matrix composites, reinforced with the WC carbide phases and austenitizing conditions

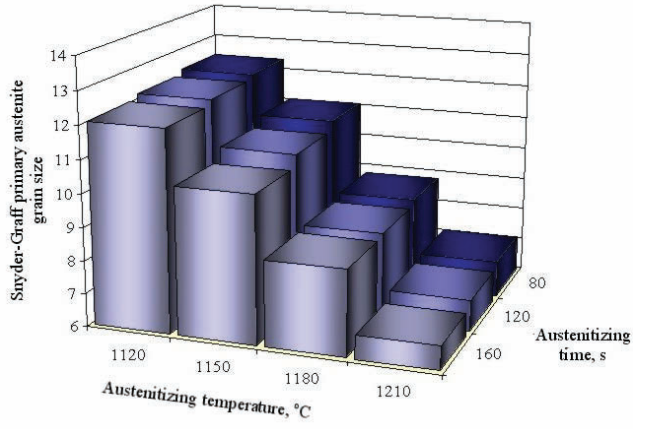

Fig. 62. Relationship between the primary austenite grain size in the substrate layer of the hardened high-speed steel matrix composites, reinforced with the WC carbide phases and austenitizing conditions

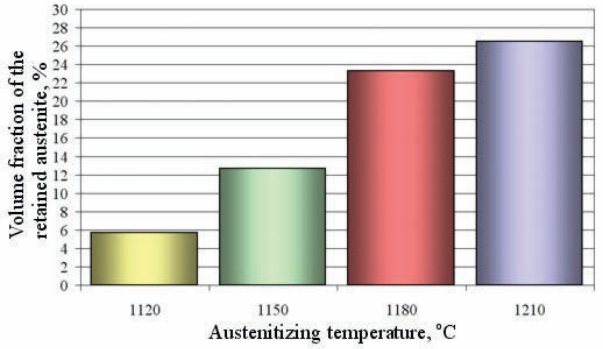

Fig. 63. Relationship between the volume portion of the retained austenite and austenitizing temperature in the substrate layer of the high-speed steel matrix composites, reinforced with the WC carbide phases austenitized for 120 s

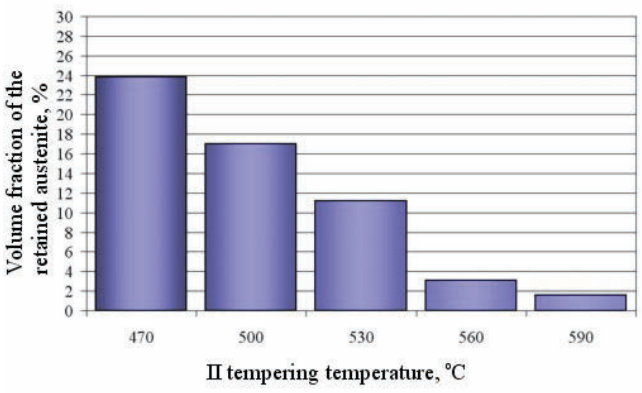

Fig. 64. Relationship between the volume portion of the retained austenite with the second tempering temperature in the substrate layer of the high-speed steel matrix composites, reinforced with the WC carbide phases hardened at temperature of 1210°C after austenitizing for 120 s

6. Summary

The following conclusions were put forward based on analysis of the investigation results for the sintered gradient cermets with the high-speed steel substrate reinforced with the vanadium- or tungsten carbides:

The conventional powder metallurgy method, consisting in the uniaxial compacting of the powder in a closed die with its subsequent sintering, makes fabrication possible of the gradient cermets with the desired structure and properties by feeding and mixing the substrate powders from the high-speed steel with the hard carbides phases, ensuring the linear change of the reinforcing phases particles portion in the substrate in the direction perpendicular to the surface, while the newly developed materials do not demonstrate cracks and delamination in the boundary zone between the layers, are characteristic of the smooth transition between the layers and demonstrate the linear change of properties.

The newly developed gradient cermets are characteristic of the multi-phase structure consisting of ferrite, primary carbides of the high-speed steel, of the MC and M_6C types, as well as – depending on the reinforcing phase type – from the tungsten- WC or vanadium carbide VC, introduced into the cermet in the form of a powder, where the MC and M_6C type carbides, depending on the sintering conditions, are uniformly distributed in the substrate or coagulate and develop forming big precipitations (ca. 2 μm) on the boundary of the primary austenite grains of the high-speed steel, moreover, the W_2C occurs in addition in the structure of materials reinforced with the tungsten carbide. The gradient cermets reinforced with the WC carbide are characteristic of a higher hardness and smaller porosity than cermets reinforced with the VC carbide. Addition of the WC carbide to the high-speed steel powder causes reduction of the sintering temperature from 1250 to 1210°C, whereas addition of the VC carbide causes increase of the sintering temperature of the materials. The MG-75HSS/25WC gradient cermets should be sintered in vacuum, at 1210°C for 30 min at the heating up/cooling rates of 5°C/min to/from the sintering temperature, which ensures material density of about 8.6 g/cm^3, surface layer hardness about 81 HRA, porosity about 2%, the substrate layer structure that does not reveal any traces of partial melting. Employment of the flowing mixture of gases causes increase of the porosity of materials.

Heat treatment of the developed gradient cermets with the core corresponding to the high-speed steel, consisting in hardening and tempering, causes the secondary hardness effect in substrate layers from the high-speed steel by about 2 to 3 HRC higher than hardness of the hardened material. Structure of the MG-75HSS/25WC materials in the hardened state is martensite with the retained austenite, M_6C and MC type carbides, primary, and also secondary ones, undissolved in the solid solution during austenitizing, as well as the WC tungsten carbides in the surface layer. The highest surface layer hardness of 71.6 HRC is characteristic of the material austenitized at the temperature of 1120°C for 120 s, hardened, and next tempered twice at the temperature of 530°C. The possibility of forming in a wide range of the surface layer hardness of the newly developed gradient cermets reinforced with the WC carbides, depending on their chemical composition and sintering conditions, offers potential for employment of these materials for cutting tools.

Acknowledgements

The authors would like to express their gratitude to the Dr M. Pawlyta, Dr K. Gołombek, Dr W. Kwasny, Dr K. Labisz, Dr G. Matula from the Silesian University of Technology in Poland and Dr E. Gordo, Prof. J. M. Torallba from University Carlos III in Madrid for their help in executing some investigation.

References

[1] L.A. Dobrzański, Principle of materials science, metallography, WNT, Warsaw, 2006 (in Polish).
[2] L.A. Dobrzański, Metal engineering materials, WNT, Warsaw, 2004 (in Polish).
[3] M. Wysiecki, Modern tool materials, WNT, Warsaw, 1997 (in Polish).
[4] L.A. Dobrzański, E. Hajduczek, J. Marciniak, R. Nowosielski, Heat treatment of tool materials, Silesian University of Technology Press, Gliwice, 1990 (in Polish).
[5] L.A. Dobrzański, E. Hajduczek, J. Marciniak, R. Nowosielski, Metallography and heat treatment of tool materials, WNT, Warsaw, 1990.
[6] M. Kupczyk, Surface engineering, WPP, Poznan, 2004 (in Polish).
[7] L. Jaworska, M. Rozmus, B. Królikowska, A. Twardowska, Functionally gradem cermets, Journal of Achievements in Materials and Manufacturing Engineering 17 (2006) 73-76.
[8] R.F. Bunshah, Handbook of Hard Coatings, William Andrew Publishing, Noyes, 2001.
[9] Y. Miyamoto, W.A. Kaysser, B.H. Rabin, A. Kawasaki, R.G. Ford, Functionally Graded Materials: Design, Processing and Applications, Kluwer Academic Publishers, Boston-Dordrecht-London, 1999.

[10] M. Schwartz, New Materials, Processes, And Methods Technology, CRC Press, Boca Raton-London-New York, 2006.
[11] J.K. Wessel, The Handbook of Advanced Materials: Enabling New Designs, John Wiley and Sons, Incorporated, 2004.
[12] K. Hodor, P. Zięba, B. Olszowska-Sobieraj, Functionally gradient materials as new challenge for modern technology, Materials Engineering 113/6 (1999) 595-600 (in Polish).
[13] K. Ichikawa, Functionally Graded Materials in the 21st Century: A Workshop on Trends and Forecasts, Kluwer Academic Publishers, Boston, 2001.
[14] B. Kieback, A. Neubrand, H. Riedel, Processing techniques for functionally graded materials, Materials Science and Engineering A362 (2003) 81-106.
[15] S. Kirihara, M. Takeda, T. Tsujimoto, Development of Ti/Ti_3Sn functionally gradient material produced by eutectic bonding method, Scripta Materialia 35 (1996) 157-161.
[16] R. Knight, R.W. Smith, Thermal Spray Forming of Materials Powder Metal Technologies and Applications, ASM Handbook, ASM International 7 (1998) 408-419.
[17] A. Maximenko, G. Roebben., O. Van Der Biest, Modelling of metal-binder migration during liquid-phase sintering of graded cemented carbides, Journal of Materials Processing Technology 160 (2005) 361-369.
[18] K. Yamagiwa, Y. Watanabe, K. Matsuda, Y. Fukui, P. Kapranos, Characteristics of a near-net-shape formed Al–Al_3Fe eco-functionally graded material produced over its eutectic melting temperature, Materials Science and Engineering A 416 (2006) 80-91.
[19] H. Yamaoka, Fabrication of functionally gradient materials by slurry stacking and sintering process, Ceramic Transactions FGM 34 (1992) 165-172.
[20] Y. Zhang, J. Han, X. Zhang, X. He, Z. Li, S. Du, Rapid prototyping and combustion synthesis of TiC/Ni functionally gradient materials, Materials Science and Engineering A 299 (2001) 218-224.
[21] L.A. Dobrzański, A. Kloc, G. Matula, Influence of forming on structure and properties of gradient materials, Materials Engineering 151/3 (2006) 584-587 (in Polish).
[22] L.A. Dobrzański, A. Kloc, G. Matula, J.M. Contreras, J.M. Torralba, Effect of manufacturing methods on structure and properties of the gradient tool materials with the non-alloy matrix reinforced with the HS6-5-2 type high-speed steel, Proceedings of the 11th International Scientific Conference "Contemporary Achievements in Mechanics, Manufacturing and Materials Science" CAM3S'2005, Gliwice – Zakopane, 2005, 223-228.
[23] L.A. Dobrzański, A. Kloc, G. Matula, J. Domagała, J.M. Torralba, Effect of carbon concentration on structure and properties of the gradient tool materials, Journal of Achievements in Materials and Manufacturing Engineering 17 (2006) 45-48.
[24] L.A. Dobrzański, A. Kloc-Ptaszna., G. Matula, J.M. Torralba, Effect of carbon concentration on structure and properties of the gradient tool materials, Founding Archives 6/21 (2006) 141-149 (in Polish).
[25] L.A. Dobrzański, A. Kloc-Ptaszna, G. Matula, J.M. Torralba, Structure and properties of the gradient tool materials of unalloyed steel matrix reinforced with HS6-5-2 high-speed steel, Archives of Materials Science and Engineering 28/4 (2007) 197-202.
[26] L.A. Dobrzański, A. Kloc-Ptaszna, A. Dybowska, G. Matula, E. Gordo, J.M. Torralba, Effect of WC concentration on structure and properties of the gradient tool materials, Journal of Achievements in Materials and Manufacturing Engineering 20 (2007) 91-94.
[27] L.A. Dobrzański., G. Matula, Structure and properties of sintered high speed-steel HS6-5-2 type formed by injection moulding, Proceedings of the 3rd Scientific Conference "Materials, Mechanical and Manufacturing Engineering" MMME'2005, Gliwice − Wisła, 2005, 203-210.
[28] L.A. Dobrzański, G. Matula, A. Varez, B. Levenfeld, J.M. Torralba, Structure and Properties of the Heat-Treated High-Speed Steel HS6-5-2 and HS12-1-5-5 Produced by Powder Injection Molding Process, Materials Science Forum 437-438 (2003) 133-136.
[29] L.A. Dobrzański, G. Matula, A. Varez, B. Levenfeld, J.M. Torralba, Fabrication methods and heat treatment conditions effect on tribological properties of high speed steels, Journal of Materials Processing Technology 157 (2004) 324-330.
[30] L.A. Dobrzański, G. Matula, A. Varez, B. Levenfeld, J.M. Torralba, Structure and mechanical properties of HSS HS6-5-2- and HS 12-1-5-5-type steel produced by modified powder injection moulding process, Journal of Materials Processing Technology 157 (2004) 658-668.
[31] L.A. Dobrzański, G. Matula, G. Herranz A. Varez, B. Levenfeld, J.M. Torralba, Influence of debinding process on microstructure and properties of HS6-5-2- HSS parts produced by powder injection molding, Proceedings of the 5th International Conference "Industrial Tools" ICIT'2005, Cejle, Slovenia, 2005, 189-195.
[32] L.A. Dobrzański, G. Matula, G. Herranz A. Varez, B. Levenfeld, J.M. Torralba, Metal injection moulding of HS12-1-5-5 high-speed steel using a PW-HDPE based binder, Journal of Materials Processing Technology 175 (2006) 173-178.
[33] A. Kloc, L.A. Dobrzański, G. Matula, J.M. Torralba, Effect of manufacturing methods on structure and properties of the gradient tool materials with the non-alloy steel matrix reinforced with the HS6-5-2 type high-speed steel, Materials Science Forum 539-543 (2007) 2749-2754.
[34] G. Matula, L.A. Dobrzański, Structure and properties of TGM manufactured on the basis of HS6-5-2, Journal of Achievements in Materials and Manufacturing Engineering 17 (2006) 101-104.
[35] G. Matula, L.A. Dobrzański, B. Dołżańska, Structure and properties of TGM manufactured on the basis of cobalt, Journal of Achievements in Materials and Manufacturing Engineering 20 (2007) 151-154.
[36] G. Matula, L.A. Dobrzański, G. Herranz, A. Varez, B. Levenfeld, J.M. Torralba, Influence of atmosphere and temperature of debinding on microstructure of HS6-5-2 HSS parts produced by Powder Injection Moulding, Proceedings of the 13th International Conference "Processing and Fabrication of Advanced Materials" PFAM XIII, Singapore, 2004, 752-761.
[37] G. Matula, L.A. Dobrzański, G. Herranz, A. Varez, B. Levenfeld, J.M. Torralba, Influence of binders on the

structure and properties of high speed-steel HS6-5-2 type fabricated using pressureless forming and PIM methods, Materials Science Forum 534-36 (2007) 693-696.
[38] G. Matula, L.A. Dobrzański, G. Herranz, A. Varez, B. Levenfeld, J.M. Torralba, Comparison of structure and properties of HS6-5-2 type high-speed steel fabricated by different powder forming methods, Proceedings of the 11th International Scientific Conference "Contemporary Achievements in Mechanics, Manufacturing and Materials Science" CAM3S'2005, Gliwice – Zakopane, 2005, 660-666.
[39] G. Matula, L.A. Dobrzański, M. Mayoral, A. Varez, B. Levenfeld, J.M. Torralba, Sintering under different atmospheres of T15 and M2 high speed steels produced by a modified metal injection moulding process, Proceedings of the International Conference "New Developments on Powder Technology", Leganes, Madrid, Spain, 2001, 1361-1368.
[40] G. Matula, L.A. Dobrzański, A. Varez, B. Levenfeld, J.M. Torralba, Comparison of structure and properties of the HS12-1-5-5 type high speed steel fabricated using the pressureless forming and PIM methods, Journal of Materials Processing Technology 162 (2005) 230-235.
[41] G. Matula, G. Herranz, A. Varez, B. Levenfeld, J.M. Torralba, L.A. Dobrzański, Microstructure and mechanical properties of T15 high-speed steels parts produced by powder injection moulding using a polyethylene based binder, Proceedings of the Powder Metallurgy World Congers and Exhibition, Vienna, 2004, 469-475.
[42] E. Klar (red.), Metals Handbook Ninth Edition 7: Powder Metallurgy, American Society for Metals, USA, 1984.
[43] R. Kieffer, W. Hotop, Powder Metallurgy and sintered materials, PWT, Katowice, 1951 (in Polish).
[44] J. Lis., R. Pampuch, Sintering, AGH, Kraków, 2000 (in Polish).
[45] J. Nowacki, Metal sintered and the metal matrix composites, WNT, Warsaw, 2005 (in Polish).
[46] E.M. Ruiz-Navas, E Garcia, E. Gordo, F.J. Velasco, Development and characterisation of high-speed steel matrix composites gradient materials, Journal of Materials Processing Technology 143-144 (2003) 769-775
[47] E.M. Ruiz-Navas, E. Gordo, E. Garcia, Development and characterisation of 430L matrix composites gradient materials, Materials Research 8 (2005) 1-4.
[48] W. Włosiński, The joining of advanced materials, WPW, Warsaw, 1999 (in Polish).
[49] C. Larsson, M. Oden, Hardness profile measurements in functionally graded WC–Co composites, Materials Science and Engineering A 382 (2004) 141-149.
[50] W. Lengauer, K. Dreyer, Functionally graded hardmetals, Journal of Alloys and Compounds 38 (2002) 194-212.
[51] W. Lengauer, K. Dreyer, Tailoring hardness and toughness gradients in functional gradient hardmetals (FGHMs), International Journal of Refractory Metals and Hard Materials 24 (2006) 155-161.
[52] M. Rosso, G. Porto, A. Geminiani, Studies of graded cemented carbides components, International Journal of Refractory Metals and Hard Materials 17 (1999) 187-192.
[53] B.L. Averbach, M. Cohen, X-ray determination of retained austenite by integrated intensities, AIME Transactions 176 (1948) 401-416.
[54] B.D. Cullity, X-ray diffraction, PWN, Warsaw, 1964 (in Polish).
[55] S. Pawlak, J. Karp, X-ray diffraction in the mw metallurgy and physical metallurgy, Proceedings of the 7th Conference "Scientifically- Technology", Gliwice, 1974, 274-283 (in Polish).
[56] J. Karp, I. Pofelska-Filip, X-ray diffraction (RIAF), Metallurgist 6 (1979) 253-269 (in Polish).
[57] X-Ray Powder Data Card File, JCPDS, ASTM, 1949-1990.
[58] PN-EN 23923-1:1998 – Metallic powders (in Polish).
[59] PN-82/H-04935 – Metallic powders (in Polish).
[60] PN-EN 1389:2005 – Ceramic technical (in Polish).
[61] L. Kukiełka, Fundamentals of Engineering Research, PWN, Warsaw, 2002 (in Polish).
[62] K. Mańczak, Experiment planning method, WNT, Warsaw, 1976 (in Polish).
[63] http://www.mathworks.com